Michele Angiolilli, Marius Eteme Minkada, Mariano Di Domenico, Serena Cattari, Andrea Belleri & Gerardo M. Verderame (2022): Comparing the Observed and Numerically Simulated Seismic Damage: A Unified Procedure for Unreinforced Masonry and Reinforced Concrete Buildings, Journal of Earthquake Engineering.
DOI: 10.1080/13632469.2022.2096721

# Comparing the observed and numerically simulated seismic damage: a unified procedure for unreinforced masonry and reinforced concrete buildings

Michele Angiolilli[a], Marius Eteme Minkada[b], Mariano Di Domenico[c*], Serena Cattari[a], Andrea Belleri[b], Gerardo M. Verderame[c]

[a] *Department of civil, chemical and environmental engineering, University of Genoa, Via Montallegro 1, 16145, Genoa, Italy;*

[b] *Department of engineering and applied sciences, University of Bergamo, Viale Marconi 5, 24044, Dalmine, Italy;*

[c] *Department of structures for engineering and architecture, University of Naples Federico II, Via Claudio 21, 80125, Naples, Italy*

michele.angiolilli@edu.unige.it, marius.etememinkada@unibg.it, mariano.didomenico@unina.it (*corresponding author), serena.cattari@unige.it, andrea.belleri@unibg.it, verderam@unina.it

The Version of Record of this manuscript has been published and is available in Journal of Earthquake Engineering
11th Jul 2022 https://www.tandfonline.com/doi/full/10.1080/13632469.2022.2096721

# Comparing the observed and numerically simulated seismic damage: a unified procedure for unreinforced masonry and reinforced concrete buildings

In this paper, a unified procedure for assessing the effectiveness of modelling strategies for existing buildings is proposed. The procedure is applied to unreinforced masonry and reinforced concrete real buildings struck by recent earthquakes. A matching index (MI) suitable to be adopted across different structural types is proposed. It aims to synthetically compare numerical outcomes with the evidence of the damage experienced by the selected case-study buildings. Results confirmed a good reliability and effectiveness of the developed numerical models (mean MI value higher than 0.70 for all the investigated case-study buildings) as well as the capability of the models in reproducing the same performance states that occurred in the real cases.

Keywords: model validation, benchmark study cases, observed damage, nonlinear dynamic analyses, masonry, precast, reinforced concrete, seismic response

## 1. Introduction

Nowadays, numerical models play a crucial role in supporting seismic performance assessments and risk analyses. Their ability to correctly reproduce the actual seismic behaviour of buildings is fundamental and, therefore, general procedures for defining the reliability of these models are needed. This reliability is strongly based on the background level of modellers, various uncertainties (e.g. the proper selection of seismic input, geometric/mechanical features of the constitutive materials, etc) as well as the capability of numerical software/framework to capture specific aspects (damage type, strength degradation, crack propagation, etc). Numerical models constitute also the tool to estimate Engineering Demand Parameters (EDP) which are correlated to the attainment of specific Limit States (LS) or losses (i.e. economic, social, usability of buildings, etc).

Within this context, the main purpose of the present research regards the validation of 3D numerical models representative of different structural typologies: UnReinforced Masonry – URM - buildings, cast-in-place Reinforced Concrete - RC - buildings and Precast reinforced Concrete – PRC – buildings. First, a global damage state is assessed for specific performance states attributed to the case-study buildings in the post-earthquake scenario, then, more specifically, the damage level is assessed at a local level. The correct reproduction of the damage severity and damage pattern is a key aspect in the seismic assessment of existing buildings, although it should be noted that it is almost impossible to numerically reproduce exactly the observed damage for each individual element of the building, as the numerical models are usually affected by both aleatory and epistemic uncertainties that can be reduced only based on the operator's expertise and accurate knowledge of the building. Thus, different methodologies are discussed in the present work aiming to quantify the damage level of the examined structural typologies as well as to investigate the reliability of the numerical models (§2). In the latter case, a cross-type procedure aimed at evaluating a Matching Index (MI) is addressed to quantify the similarity between the observed and simulated damage state of a damaged building.

The proposed method is applied to five existing case-study buildings (three URM and two reinforced concrete buildings (i.e. one RC and one PRC)) representative of the existing Italian building stock and subjected to different damage states after recent seismic events. The selected buildings were modelled following the modelling strategies adopted for the archetype buildings investigated within the RINTC (*Rischio Implicito delle strutture progettate secondo le NTC* (in Italian), *Implicit Risk of structures designed according to NTC*) project. The project, funded by the Italian Civil Protection Department, aimed at assessing the implicit seismic risk of code conforming (RINTC project, Iervolino et al. 2018) and existing buildings (RINTC-e project, to which this Special Issue is dedicated, and illustrated in Iervolino et al. 2021).

The criteria adopted to select the case-study buildings are discussed in detail in §3 while the specific results of URM and both RC and PRC case studies are described in §4, and §5 respectively. The effectiveness of the modelling strategies and the capacity assessment methodologies were investigated through the capability of the numerical models in reproducing both the global damage state representative of specific performance states of the buildings and the observed damage for each structural element (i.e. by the estimation of the MI).

The relevance of the present research work is threefold: i) the validation of the consistency of the performance states for different structural typologies adopted within the RINTC-e project and the associated adopted modelling strategies; ii) the proposal of a general methodology for evaluating the reliability of numerical models of existing buildings, through the application to different structural typologies; iii) the provision of a valuable benchmark study of real damaged buildings struck by earthquakes that can be adopted as a reference in other practical studies.

## 2. Benchmark: needs and proposed methodology

The relevance of the reliability of numerical simulations is testified by the increasing effort of various literature works in defining benchmark study cases, proposed to be replicated also by other researchers (e.g. Cattari and Magenes 2021, Parisse et al. 2021 for URM and Haselton and Deierlein 2005 for RC). Other benchmarking studies have been occasionally carried out through blind prediction of experimental campaigns (e.g. Mendes et al. 2017, SERA Project 2017, Esposito et al. 2019 for URM and Richard et al. 2016, Furtado et al. 2018 for infilled RC); surely, experimental campaigns performed on shaking tables constitute a valuable and irreplaceable resource to validate models (e.g. Magenes et al. 2014, Senaldi et al. 2020 for URM, Lourenço et al. 2016, Yeow et al. 2020, Kajiwara et al. 2021 for RC, Schoettler et al. 2009, Xiao et al. 2015, Zhang et al. 2019 for PRC buildings).

The above-mentioned campaigns, among others, showed the major criticism associated with a reliable modelling and performance assessment of real structures. For example, for URM, it was found that defining a specific failure mode for each element becomes more conventional and difficult passing from simplified to more refined models, especially in the case of axial load values where a transition zone between the prevalence of the flexural failure and the shear failure occurs (Castellazzi et al. 2021). The higher scatter between numerical results was also due to significant differences among approaches in considering in-plane (IP) and combined in-plane and out-of-plane (IP+OOP) mechanisms, which are better captured by refined models. In addition, those tests confirmed the benefit of floor-to-wall and roof-to-wall connections as well as the good quality of constitutive materials in preventing the local OOP (e.g. Magenes et al. 2014).

Regarding existing RC buildings, the previous benchmarking campaigns further highlighted the main evidence of recent earthquakes (e.g., L'Aquila 2009): a severe structural damage at both local and global level is due to potential brittle failure of vertical members (i.e., columns), while usability-preventing and loss-procuring damages are more frequent and mainly related to the damage of non-structural elements (i.e., masonry infill walls) (Ricci et al. 2011, Braga et al. 2011, Vicente et al. 2012). In addition, for PRC buildings, the previous studies showed the importance of defining an appropriate model for the connections between structural and non-structural (i.e., cladding panels) elements, which is crucial for a reliable estimate of the seismic damage of buildings (Ercolino et al. 2016, Magliulo et al. 2021, Gajera et al. 2021, Bressanelli et al. 2021).

The benchmarking of the RINTC-e project was carried out considering case studies selected from real buildings struck by recent earthquakes. This choice is motivated by the fact that technological limitations of shaking-table facilities often impose strong oversimplifications with respect to the actual complexity of real buildings, also introducing the need to define scaling factors and apply similitude laws due to size-effect (Croci et al. 2010, Senaldi et al. 2020, Bazant and Planas 1997, Angiolilli et al. 2021a). The proposed methodology, used for the benchmarking of the RINTC-e project, involves the following key aspects to define the effectiveness of the numerical model, as schematically depicted in Figure 1.

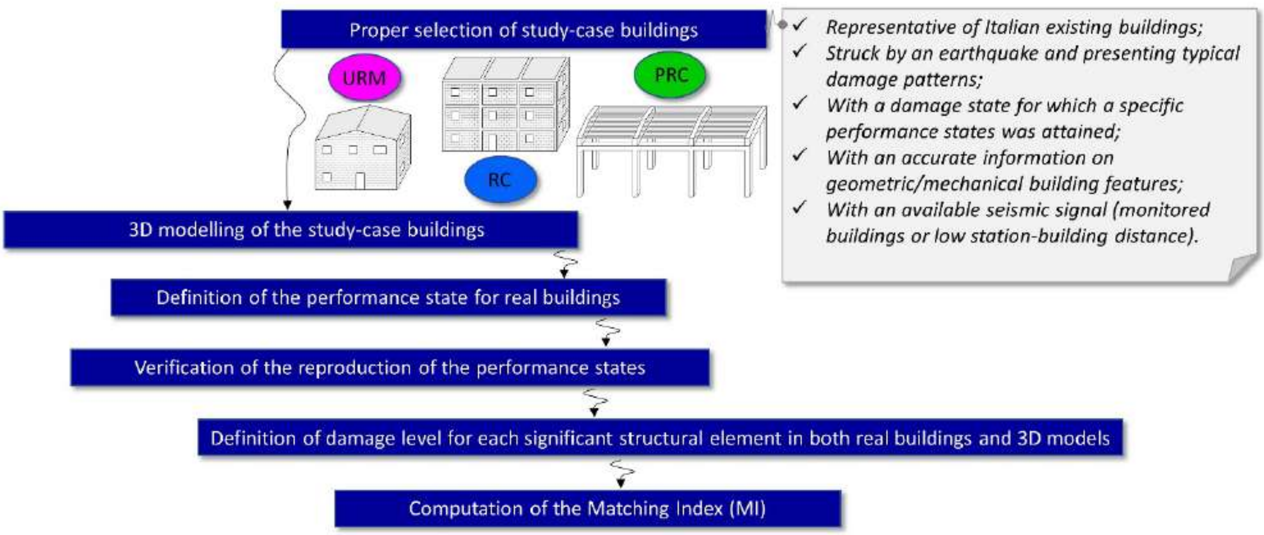


Figure 1. Schematic layout of the methodology proposed in this work to validate numerical simulations.

First of all, a proper selection of case-study buildings within a benchmark work is the primary goal required to provide a reliable insight for the nonlinear analyses. Therefore, the selected buildings should present both geometric and structural features typical of the considered existing stock (e.g. 2-3 storeys URM buildings, 3-5 storeys RC buildings or single-story PRC structures widely spread in Italy) and they should be characterized by a relevant seismic vulnerability highlighted by past earthquakes (herein: Molise 2002, L'Aquila 2009, Emilia 2012, Central Italy 2016-2017). Among those structures, the ones showing selected damage states should be preferred: indeed, the damage performance state achieved in a building allows testing the reliability of 3D models within a low-level of nonlinearity, whereas the collapse performance state allows testing the reliability of a high-level of nonlinearity. Within the RINTC-e project, two performance states were considered: the Global Collapse (GC) and the Usability-Preventing Damage (UPD). More specifically, the UPD corresponds to the achievement of specific damage levels (DL) attained in the structural elements assessed by nonlinear analyses: for example, the occurrence of DL2 for 50% of the significant elements or the achievement of DL3 for at least one element. The GC was instead considered achieved when 50% of the residual strength in the softening behaviour of the global response of the structure occurred or when a specific ultimate value of a given Engineering Demand Parameter (EDP) was attained in the primary structural elements. Note that multi-criteria approaches could be also applied as specified better for each structural typology. Obviously, these performance states can be also defined for real structures on basis of the surveyed damage, for example by adopting the general criteria based on EMS98 and proposed in (Dolce et al. 2019, Rota et al. 2008) that combine the DL attained at element scale with their diffusion on the building.

The current benchmarking was carried out considering some of the relevant seismic vulnerabilities experienced in the selected structural typologies (Table 1). The typical damage failures that occurred to existing URM buildings struck during recent earthquakes can be found, for example, in (Augenti and Parisi 2010, D'Ayala and Paganoni 2011, Indirli et al. 2013, Cattari et al. 2012, Penna et al. 2014, Sorrentino et al. 2019) and can be divided into two main categories, such as the IP behaviour and local mechanisms, mainly associated with out-of-plane OOP failures of single parts. When OOP mechanisms are prevented, the IP behaviour is observed in URM buildings, mainly activating the shear capacity of the main structural elements of the vertical wall (i.e. piers or spandrels) (e.g. De Felice 2011, Morandi et al. 2019). On the other hand, the combined role of IP and OOP mechanisms can strongly reduce the seismic performance of buildings (Angiolilli et al. 2021b).

Regarding RC structures, during an earthquake, the structural members experience a concentration of rotational ductility demand at their ends (Ricci et al. 2011) and a possible brittle shear failure, especially in substandard vertical members characterized by limited shear reinforcement (Verderame et al. 2011). In past earthquakes, a significant damage was observed particularly in non-structural elements, both infill masonry panels and internal partitions (Ricci et al. 2011, Braga et al. 2011, Vicente et al. 2012, Manfredi et al. 2014, Masi et al. 2019), whose assessment is paramount for a comprehensive seismic performance evaluation of this structural typology from both a safety and economic loss point of view (Di Ludovico et al. 2017a, 2017b).

Considering PRC structures, a significant number of single-story industrial buildings showed several local roof collapses during past earthquakes (Belleri et al. 2015a; Casotto et al. 2015; Ercolino et al. 2016; Demartino et al. 2018; Eteme Minkada et al. 2021) mainly due to inadequate beams-columns and beams-roof elements connections, typically relying on friction for regions not classified as seismic prone at the time of construction. Other seismic vulnerabilities are related to local failures of the structural components or of non-structural elements (Savoia et al. 2012; Toniolo and Colombo 2012; Bournas et al. 2014; Magliulo et al. 2014; Belleri et al. 2015a; Minghini et al. 2016; Nastri et al. 2017; Palanci et al. 2017; Sousa et al. 2020).

Table 1. Recurring damage selected for the benchmarking of the considered structural typologies.

| | URM | RC | PRC |
|---|---|---|---|
| Typic/critical damage | Flexural/shear damage to load-bearing wall and OOP local mechanisms | Brittle failure of shear-sensitive members; infill damage | Fall of roof elements due to the poor connecting system with the substructure |

To reduce the aleatory uncertainties, the study cases were selected among the buildings with accurate documentation on the real damage, architectural and construction drawings as well as non-destructive or destructive tests on the constituent materials. In addition, the availability of the seismic input or a low site-station distance was another criterion of study case selection.

Once the accurate selection of the case-study buildings is performed, the following step regards the development of 3D numerical models adopting software/frameworks suitable to capture the selected failures. The key aspects of the numerical models adopted in this work are described in detail in Section 4.1 for URM and Section 5.1 for RC and PRC.

Then, the final step of the benchmark work is the reproduction of a global damage state comparable with that occurred in the study case buildings through the verification of specific performance levels, either damage or collapse. Only when this condition is attained, a precise comparison between the numerical and the observed damage level that occurred for each significant structural element could be performed. The reliability of the developed 3D models is assessed through the computation of the Matching Index (MI) as described in the following section.

## 2.1. The matching index as a cross-type proposal

In this work, the reliability of the results of non-linear dynamic analyses (NDA) and, therefore, the effectiveness of the numerical models in capturing the real damage state of the investigated buildings is represented through the MI. This index can be computed by assuming firstly a reliability factor $MI_E$ (equal to 1, 0.5, 0.25 or 0) for each significant E-*th* structural or non-structural element (e.g. piers/spandrels or, more generally, walls, for URM, columns/beams/infills for RC or roof elements for PRC) of the investigated building based on the similarity level between the observed and the simulated damage level that occurred ($DL_{E,OBS}$ and $DL_{E,SIM}$, respectively). Note that herein DL was set on five levels (i.e. DL1 to DL5), as proposed in the EMS98 scale (although the physical meaning varies passing from global scale, for which EMS98 was conceived, to the scale of the single element).

Therefore, it is possible to compute the overall MI of the investigated building through the following equation:

$$MI = \frac{\sum_1^{n_E} MI_E}{n_E} \tag{1}$$

where $n_E$ is the total number of the significant structural elements. Hence, MI is a continuum variable ranging from 0 to 1 (or 100%, representing the case in which the simulated damage of each structural element corresponds exactly to the real damage). The authors suggest to consider each significant structural element, including those characterized by null $DL_{E,OBS}$, for the computation of MI to better investigate the reliability of the simulation. For example, if $DL_{E,OBS}$ is null for a specific element and, at the same time, the simulations led to a certain damage (and vice-versa), the MI is negatively affected. Note that Cattari et al. (2022) have proposed an application of the MI method to drive parametric analyses to get the most accurate numerical model for a URM building.

The criteria adopted to define the damage state to the structural elements may differ across the different structural types. However, the different procedures to define $MI_E$ must be consistent among them to establish a coherent way to compare the reliability of different adopted models. In this study, two possible practical ways to define $MI_E$ are proposed and depicted in Table 2. They consist of a “deterministic” and “probabilistic” method depending on the nature of the DL thresholds.

Table 2. Two criteria proposed for the evaluation of the reliability factor $MI_E$ for each significant E-*th* structural element.

| Criterion 1 | Criterion 2 | $MI_E$ |
|---|---|---|
| If $\lvert\Delta DL_{E,SIM-OBS}\rvert \leq 0.75$ | If the most probable $DL_{E,SIM}$ correspond to $DL_{E,OBS}$ | 1 |
| If $0.75< \lvert\Delta DL_{E, SIM-OBS}\rvert \leq 1.5$ | If the most probable $DL_{E,SIM}$ is not equal to $DL_{E,OBS}$ but its probability of occurrence is lower than 50% and, contemporarily, the second more probable $DL_{E,SIM}$ corresponds to $DL_{E,OBS}$ | 0.5 |
| If $1.5 < \lvert\Delta DL_{E, SIM-OBS}\rvert \leq 2$ | If the most probable $DL_{E,SIM}$ is not equal to $DL_{E,OBS}$ and, contemporarily, the second more probable $DL_{E,SIM}$ correspond to $DL_{E,OBS}$ | 0.25 |
| If $\lvert\Delta DL_{E, SIM-OBS}\rvert > 2$ | Otherwise | 0 |

In particular, the deterministic criterion – defined in the first column of Table 2 - can be adopted when the simulated damage state that occurred for each structural element can be associated directly with the achievement of a specific EDP (displacement, chord rotation or drift) thresholds, assumed as deterministic. This is mainly due to the possibility of considering EDP-DL relations within the software/framework adopted for the NDAs. Hence, for each element, it is possible to define a specific (deterministic) $DL_{E, SIM}$ based on the overcoming of specific numerical DL thresholds (defined basedon the experimental evidence), as depicted in Figure2a. For example, the constitutive laws adopted for pier and spandrel elements of URM case-studies (Section 4.1) are characterized by shear-drift characteristic points corresponding to different damage states, allowing to evaluate directly the "numerical" damage on each structural element. The same applies for structural members in cast-in-place RC structures, for which Del Gaudio et al. (2018) assumed that the damage state of a structural member can be associated with the characteristic points of its moment-chord rotation response (cracking, yielding, post-yielding). Moreover, for the PRC case, the $DL_E$ can be defined as a function of the relative displacement demand, Δ, in the beam-roof element connections. Those EDP can be directly obtained for each structural element from NDAs. Therefore, for both URM and PRC cases, one can directly compare the difference between the simulated and observed DL that occurred for them (i.e. $\Delta DL_{E,SIM-OBS}$) and, therefore, define an overall MI of the investigated building by adopting Eq. (1). Figure 2a shows an idealized backbone curve obtained for a specific E-*th* in the NDA that led to a specific $DL_{E,SIM}$ exceeding a fixed EDP threshold associated with a specific DL. That $DL_{E,SIM}$ (in the example of the figure equal to 3) is compared to the $DL_{E,OBS}$ (in the example equal to 2) determining a $MI_E$=0.5 for that element.

In general, positive or negative values of $\Delta DL_{E,SIM-OBS}$ indicate overestimation or underestimation of the simulated damage, respectively. Obviously, the lower the $|\Delta DL_{E,SIM-OBS}|$ value, the higher the reliability of the simulation and, therefore, the $MI_E$ value. Low values of $\Delta DL_{E,SIM-OBS}$ can also indicate possible unexpected localization of the simulated DL as well as underestimation of the DL on individual structural elements, suggesting how the definition of their geometric/mechanical features or constructive details were not properly considered in the numerical models.

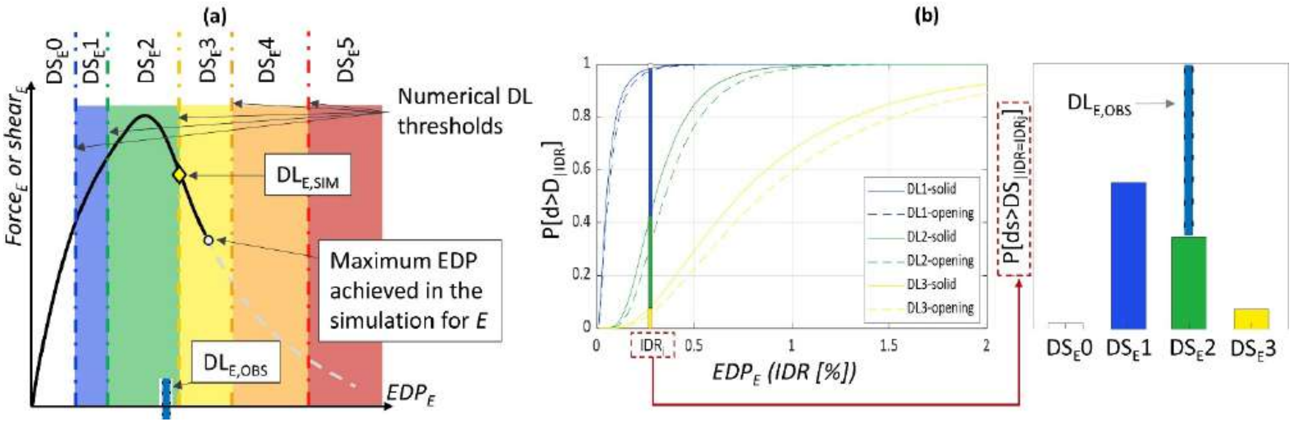


Figure 2. a) criterion n.1 of Table 2: backbone curve of a specific element obtained from the simulation leading to a $DL_{E,SIM}$; b) criterion n.2 of Table 2: Fragility curves for different DLs for clay hollow brick masonry infills, with and without openings (on the left) and indication of the respective probability of occurrence for a given IDR specifically for the case without openings (on the right).

Alternatively, it is possible to apply the probabilistic criterion - defined in the second column of Table 2 - when the thresholds of the numerical damage state is established passing through proper fragility curves. In that case, the fragility curves are known from other empirical/numerical studies and indicate the most probable damage level that occurred for the elements as a function of specific

EDPs as well as a function of other conditions, such as material type and geometric/mechanical characteristics of the elements. Therefore, if the simulations lead to the most probable DL suggested by those fragility curves, the $MI_E$ value is equal to 1. Otherwise, $MI_E$ is lower than 1 and depends on the proximity to the second more probable DL. For example, for the RC case, drift-based fragility curves for masonry infill walls in RC frames proposed in (Del Gaudio et al. 2019, Del Gaudio et al. 2021) were assumed as reference. Those fragility curves were based on experimental tests and defined for both infills with and without openings and, among them, for infills made of different materials (hollow clay bricks, concrete blocks, etc.). Among clay hollow brick masonry infills, specific fragility curves were also defined based on the infill height-to-thickness slenderness ratio. For each typology, fragility curves were defined with reference to four different DLs and express the probability that the damage level, d, exceeds the damage threshold D associated with a certain DL given the value of the maximum IDR demand, as shown in Figure 2b. In the example reported in that figure, the most probable $DL_{E,SIM}$ is equal to 1 with a probability of occurrence of about 60%, whereas the second most probable $DL_{E,SIM}$ is equal to 2. Since that $DL_{E,OBS}$ is equal to 2, $MI_E$ is equal to 0.25.

Note that, at present, the second criterion is not applicable to URM because no robust DL-damage correlation is yet available for it. Indeed, despite the increasing availability of experimental datasets regarding EDPs (e.g. Beyer and Dazio 2012, Vanin et al. 2017, Graziotti et al. 2018, Rezaie et al. 2020), they are mostly correlated to only specific damage levels (e.g. at the collapse or near-collapse) or limit states associated with specific conditions of Codes.

## 3. Selection of case-study buildings and description of their real seismic response

### 3.1. Overview

The methodology described in the previous section is here applied to case-study buildings belonging to the Italian building stock struck by recent seismic events. In particular, they consist of three URM structures and two reinforced concrete structures (one cast-in-place with infilled frames RC, and one made with PRC elements.). It is worth noting that the proposed methodology and the benchmarking investigation have been promoted within the RINTC-e project, therefore, the selection of the case-study structures was particularly driven by the need to validate the finite element model strategies for existing buildings (i.e. substandard not code-conforming) similar to those studied within RINTC-e project in terms of structural typology and construction age.

A brief discussion on the selected case-study structures is reported in the following. More details are provided in Section 3.2, Section 3.3 and Section 3.4, for URM, RC and PRC structures, respectively. For these structures, a quite accurate documentation regarding geometry, structural detailing and adopted materials were available.

In particular, the three selected URM buildings, which were built in the 1920s-1960s, were characterized by different masonry typologies and plan configurations representing the most widespread ones in the Italian existing URM stock. Note that, two of them were also monitored during the earthquakes ensuring the most accurate seismic signal for the NDAs.

The two selected reinforced concrete structures (for which the same modelling approach was adopted), were built in the 1970s and consist of an infilled RC residential multibay multistorey building (cast-in-place) and a one-storey PRC building. The RC structure showed the typical damage pattern observed for residential buildings in the aftermaths of the 2009 L'Aquila earthquake, with null/low damage to structural members and widespread moderate damage to nonstructural parts, namely to exterior infill walls (Del Gaudio et al. 2019, 2020). On the other hand, the PRC building, showed the typical damage pattern observed for this structural typology after Emilia earthquake, with moderate damage to structural members and severe damage to roof elements due to their fall during the earthquake. Hence, the two selected reinforced concrete structures cover a quite wide range of potential structural damage (from null to moderate) and nonstructural damage (from light/moderate to severe).

Figure 3 depicts the location of the investigated case-study buildings and that of the seismic actions adopted in the numerical simulations. In particular, those seismic events consist of the 2009 L'Aquila (for the RC building), the 2012 Emilia (for the PRC building and one of the URM building) and the 2016/2017 Central Italy earthquake (the other two URM buildings).

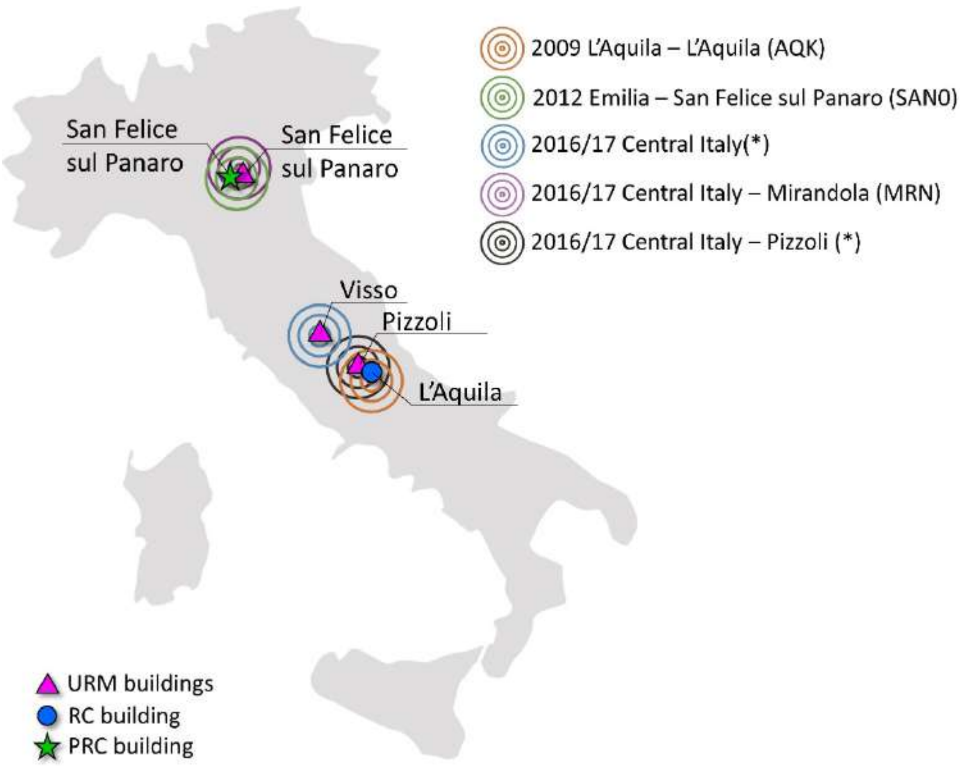


Figure 3. Location of the five investigated case-study buildings in the Italy map with indication of the seismic event and the ID earthquake (*monitored structure).

The main data on the seismic inputs adopted in the NDAs of the five case-studies are reported in Table 3.

Table 3. main features of the seismic events that struck the case-study buildings (*monitored structure; $M_L$: Richter Magnitude; R-epi: epicentral distance).

| **structural typology** | **ID eartquake** | **Seismic event** | **$M_L$ [-]** | **PGA [g]** | **R-epi [km]** | **station-building distance [km]** |
|---|---|---|---|---|---|---|
| URM | San Felice Sul Panaro (SAN0) | 2012 Emilia | 5.8 | 0.221 | 4.7 | 0.3 |
| URM | Pizzoli (-) | 2016/17 Central Italy | 5.4 | 0.112 | - | 0.0* |
| URM | Visso (-) | 2016/17 Central Italy | 6-5.9-6.1 | 0.334-0.476-0.301 | - | 0.0* |
| RC | L'Aquila (AQK) | 2009 L'Aquila | 6.1 | 0.28 | 5.6 | 6.0 |
| PRC | San Felice Sul Panaro (SAN0) | 2012 Emilia | 5.8 | 0.221 | 4.7 | 1.1 |
| PRC | Mirandola (MRN) | 2012 Emilia | 5.9 | 0.264 | 16.1 | 6.9 |

The San Felice sul Panaro URM case-study building was selected for its proximity (about 300 m) to the accelerometric monitoring system, ensuring a good reliability of the seismic input. For that building, the SAN0 seismic record of May 29th was taken into account for the NDA because it generated the highest damage level to the structure. Note that the same record was also used as seismic input for the NDA performed on the San Felice's PRC case together with the MRN one recorded on 20th May. The other two URM study cases are monitored buildings damaged by the 2016/17 seismic events: the Pizzoli's URM building (instrumented since 2009, Spina et al. 2019) was mainly damaged on 18th January 2017. Note that in (Degli Abbati et al. 2021) the damage accumulation effect was investigated, showing a negligible effect of the previous mainshocks on that structure. On the other hand, the Visso's URM building was located in the near field region of the 2016 Central Italy seismic sequence and was struck by three mainshocks with $M_L$ equal to 6.0, 5.9 and 6.1 on 24th August, 26th October and 30th October 2016, respectively. Those consequent seismic actions, recorded by a monitoring system, led to an important damage accumulation effect on the building and, therefore, were used as sequential seismic inputs in the NDAs.

Finally, the RC case-study building located in L'Aquila was struck by the mainshock of the 6th April 2009. The nearest record from that structure is provided by AQK station at a distance equal to 6 km. Hence, a simulated record was also adopted for the NDAs: the simulated record (Evangelista et al. 2017) corresponds to the "Monitor 3" virtual station.

### 3.2.URM buildings in San Felice Sul Panaro, Pizzoli and Visso

The selected study cases comprise 3 URM existing buildings built in the 1920s-1960s and struck by recent earthquakes, i.e. the 2012 Emilia and 2016-17 Central Italy earthquakes. In particular, the study-case buildings (illustrated in Figure 4) are located in San Felice sul Panaro (MO, synthetically called "San Felice" in the following), Visso (MC) and Pizzoli (AQ) municipalities. All the study cases were selected because they showed a prevailing global response (the so-called "box behavior") during the earthquakes, with an activation of the IP behavior of the load-bearing walls and a damage concentration in piers (i.e. the vertical resistant elements) and spandrels (i.e. the parts of walls between two vertically aligned openings). Two of them also presented the activation of local OOP mechanisms but concentrated in small portions of the buildings (a part of an external façade in both cases). Furthermore, as introduced in section 2, the study cases were selected because they were characterized by different damage level scenarios, from slight to severe damage, representing a fundamental aspect for a more comprehensive validation of the simulation of URM buildings.

The selected URM buildings were characterized by different masonry typologies representing the most widespread ones in the Italian existing URM stock, i.e. from cut stone with horizontal courses made of clay brick units (Pizzoli's case) or hewn stone (Visso's case) to regular clay brick (San Felice's case). The buildings are also characterized by different plan configurations: squared for the San Felice'case; "T-shaped" for the Visso's case; and "C-shaped" for the Pizzoli's case.

The detailed description (geometry, material and observed damage) of the San Felice's building, Visso's school and Pizzoli's school are reported in (Cattari and Lagomarsino 2013a) (Brunelli et al. 2021) and (Cattari and Magenes 2021, Degli Abbati et al. 2021), respectively.

In particular, the Visso's building was characterized by the highest damage state, with respect to the other study cases, overall classifiable as heavy (damage grade 4 according to EMS98). Damage was mainly concentrated in piers by the occurrence of diagonal cracks, although severe damage occurred also in spandrels. The building was affected by relevant damage accumulation phenomena, being hit by three shocks with a magnitude higher than 5.5 (Brunelli et al. 2021). After the shock of 24th August 2016 the building already suffered an appreciable damage (characterized only by IP damage of walls), then strongly aggravated by the second shock that occurred in 26$^{th}$ October 2016 after which a partial overturning of a back façade caused the collapse of some portions of walls of the upper floors. Furthermore, some diaphragms of both the ground and first levels suffered partial collapses after this shock. The high damage level observed for the building was also related to site amplification and soil-structure interaction phenomena, as already investigated in (Brunelli et al. 2021).

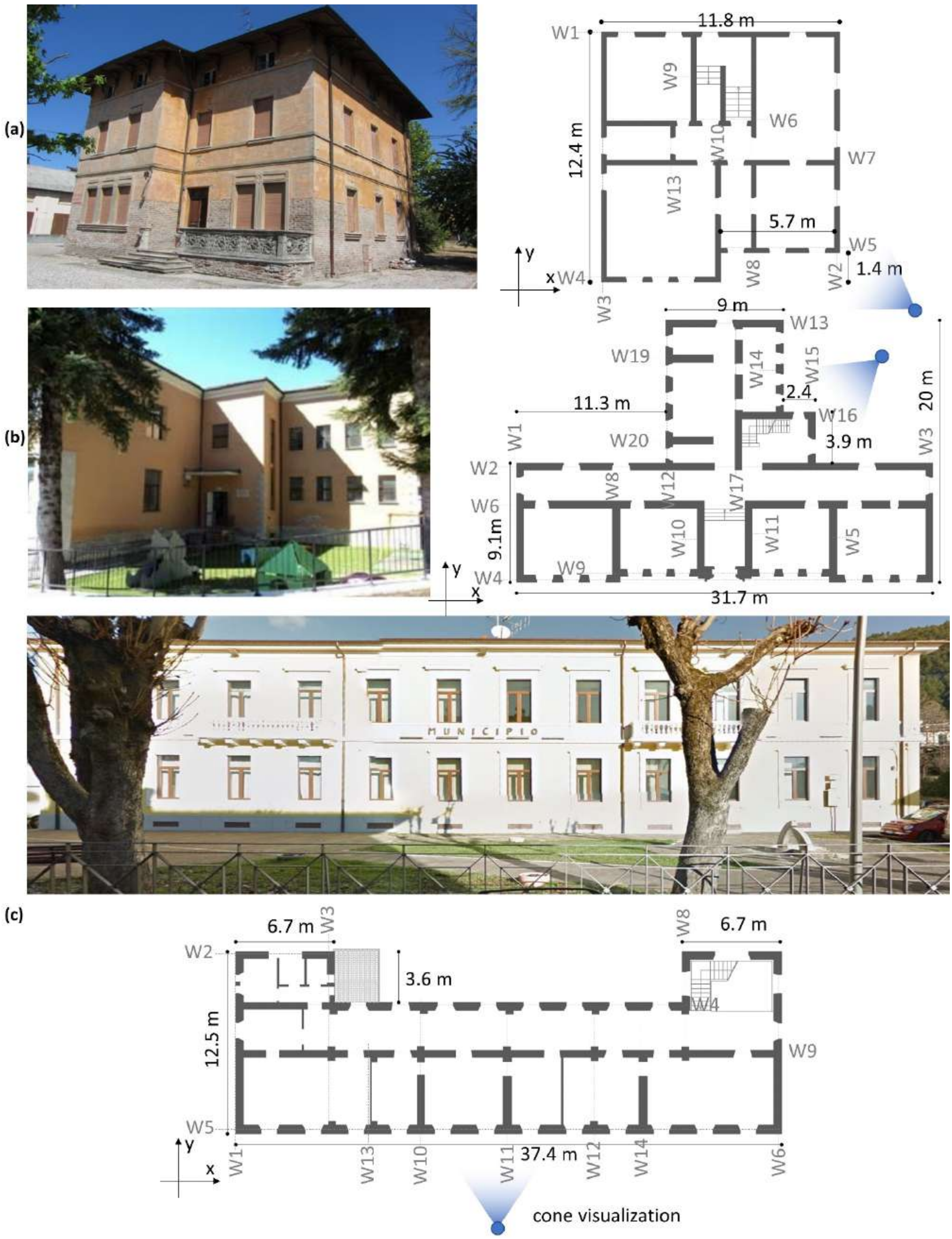


Figure 4. External view and plan of the ground floor of the: a) San Felice sul Panaro's building; b) Visso's School; c) Pizzoli's building (dimensions not in scale for sake of clarity). The ID of the walls (W) are also indicated.

Differently from the other study cases, for the Visso's case an almost uniform damage concentration between the floors was observed. Indeed, the other two buildings (especially the San Felice's building) showed a damage concentration on the piers of the ground floor, presenting both diagonal and flexural cracks on these elements.

The S. Felice's building showed a severe damage concentrated on the spandrels with the occurrence even of the lintel collapse at the upper floor; only a slight-moderate damage was instead observed for the piers. Furthermore, a severe damage level in a minor portion of the diaphragm at the first floor was observed. In general, that building was affected by a moderate damage level (damage grade 2 according to EMS98).

Concerning the Pizzoli's building, it exhibited a slight-moderate damage (damage grade 2 according to EMS98) after the 2016/2017 Central Italy earthquake, in particular referring to the event of 18th January 2017 (the closest epicenter to this building). The damage mainly occurred on pier elements of the ground floor through the development of slight diagonal/flexural cracks..

The adopted procedure requires to assign a DL (set on five levels) to structural elements - $DL_P$ for piers, $DL_S$ for spandrels - although the physical meaning varies passing from one scale to another, and it is possible to combine them to define the average DL of each i-th wall of the building ($DL_{W,i}$). Note that piers are the main resistant elements carrying vertical loads and equilibrating the horizontal forces produced by the earthquake, whereas spandrels are usually considered as secondary elements affecting the boundary conditions of piers (by allowing or restraining end rotations). Hence, from a structural point of view it is much more relevant reproducing the correct damage especially in the piers. Therefore, a weight factor ($W_W$), was introduced and assigned to each k-th pier on the basis of the influence that they have on the vulnerability of the entire building (it can depend on its stiffness or sectional area, planimetric configuration, etc.). In this paper, $W_W$ was evaluated from the results of the NSAs carried out on the Equivalent Frame EF models. On the other hand, $DL_S$ was treated as an additional factor influencing the $DL_W$ through the application of a coefficient $\alpha_{S,i}$ (varying from 0 to 1) representing the rate that possible damage on spandrels has with respect to that of the entire wall. Please refer to Cattari and Angiolilli (2022) for more details.

Figure 5 illustrates an example of the DL assignment to the Visso's piers (consistent with the damage that actually occurred at the end of main shocks and more precisely after the 30th October 2017) together with the formulation adopted to compute the $DL_W$ for each *i*-th wall of the building.

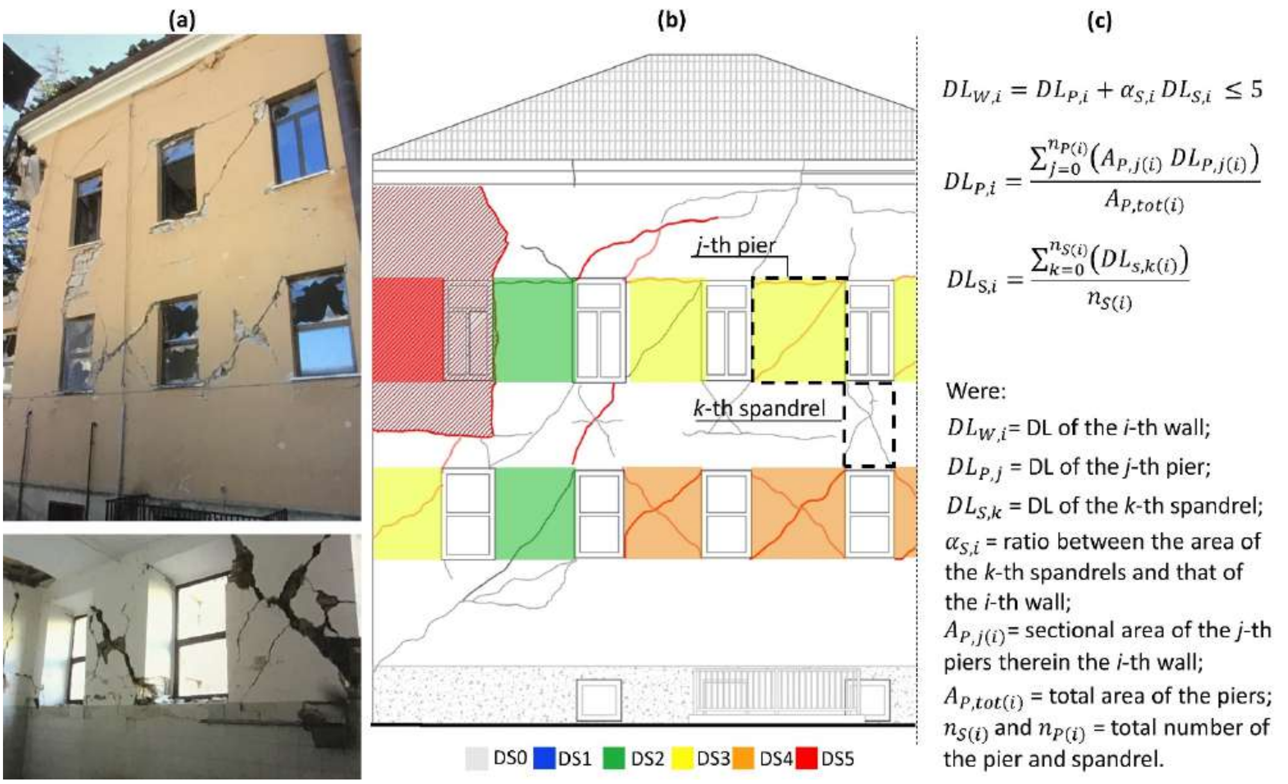


Figure 5.(a) external and internal view of the real damage (Visso's study case at 8th December, 2012); (b) interpretation and assignment of DL to the piers of the URM panels based on both internal and external wall damage depicted in (a); (c) calculation of the wall damage $DL_W$.

Figure 6 summarizes the information about the extension of the real DL that occurred for the walls as well as piers and spandrels of the three study cases.

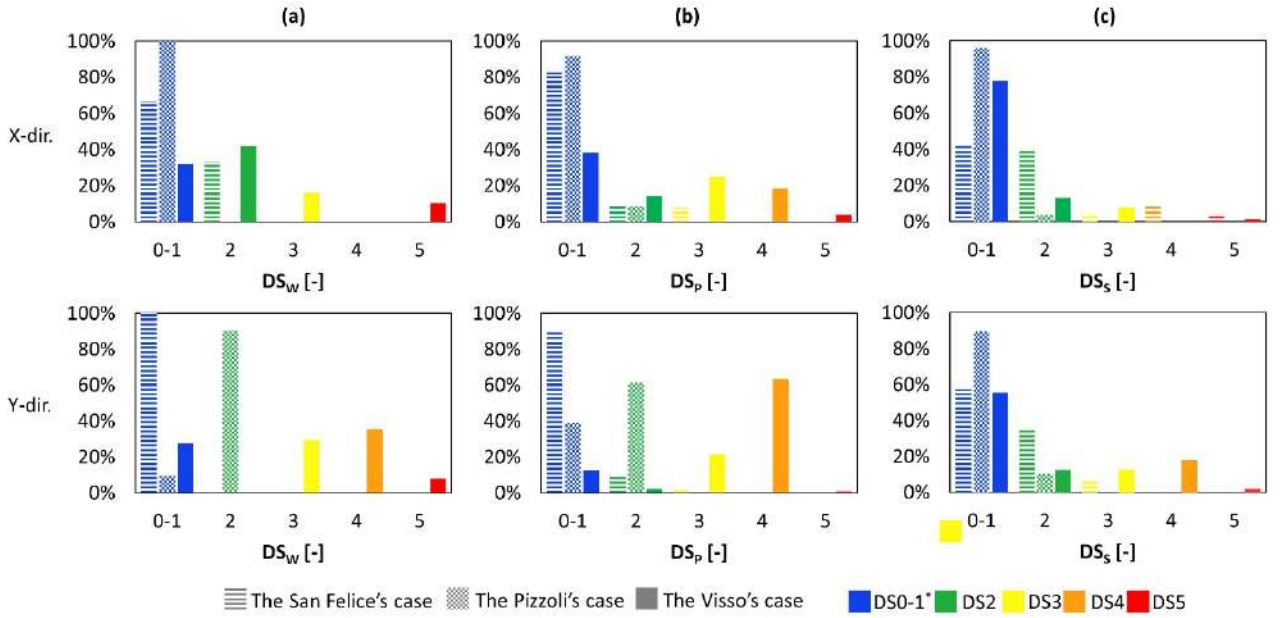


Figure 6. DL extension (in percentage) observed for walls (a), piers (b) and spandrels (c) of the buildings along their two main direction (* it is almost impossible to distinguish DS0 and DS1 by visual survey).

Finally, it is important to point out that the damage to diaphragms was neglected in the procedure for the assignment of $DL_G$ because, as discussed in Cattari and Angiolilli (2022), in the case of real buildings struck by earthquake, diaphragm weaknesses may be conventionally considered in the wall damage level.

Furthermore, damage to nonstructural elements (infill walls, false ceilings) was not taken into account in the procedure because, although these elements can have a primary influence on the performance response of other structural typologies (like the RC or PRC ones), their damage does not significantly affect the structural performance or economic losses of masonry buildings (e.g. Ottonelli et al. 2020).

### 3.3. RC building in L'Aquila

The case-study building of Figure 7 (see Cosenza et al. 2018) is a three-storey infilled RC structure framed in the transverse direction. It was built in L'Aquila municipality in the early '70s on a horizontal soft soil (i.e., T1 topography and type B soil according to current (Eurocode 8, 2004) classification). The building was designed for residential use according to the seismic provisions given by (Law n. 1684, 1962) and the structural details given by (D.M. 30/05/1972, 1972). The transverse direction of the building is rotated by 40° with respect to North-South direction.

Plain bars were used as the longitudinal and transverse reinforcement. All columns have (30×50)cm$^2$ section, with 8 longitudinal rebars (3 rebars per each side) with diameter of 14 mm and stirrups with diameter of 6 mm at 20 cm spacing. Except for the roof, all beams have (30×50)cm$^2$ cross-section with a variable number of longitudinal rebars with diameter equal to 14 mm and stirrups with diameter equal to 6 mm at 20 cm spacing. At beam ends, the transverse reinforcement is integrated with the presence of bent-up bars. The above description is referred to beams designed to support seismic and gravity loads, i.e., those realized along transverse direction; however, in the longitudinal direction, some wide beams with (50×20)cm$^2$ section are present. In accordance with the code prescriptions of that time, beam-column joints are not provided with any transverse reinforcement. The building is provided with 20 cm-thick concrete-and-hollow brick floors, with a 4 cm-thick concrete slab. Hence, it can be assumed that floor slabs have a rigid behaviour. The staircase is made of a 16 cm-thick waist slab.

Exterior infill walls were realized with two-leaf clay hollow brick masonry panels with thickness equal to (8+12) cm. Unfortunately, mechanical properties of masonry are not known, hence they were assumed to be equal to those already adopted to model the infill walls of the archetype buildings analyzed in the project with construction period and structural typology consistent with the case-study structure. Interior partitions were realized with 10 cm-thick infill panels; however, consistently with the approach adopted for modelling the archetype buildings of RINTC-e project, they were not considered in structural analysis.

Structural material properties were determined by testing concrete core samples and steel rebars with diameter of 6 mm. The resulting average concrete compressive strength is equal to 16.7 N/mm$^2$; the resulting average steel yielding stress is equal to 403 N/mm$^2$. Concrete elastic modulus was determined based on Eurocode 2 (2004) formulation and is equal to 25677 N/mm$^2$.

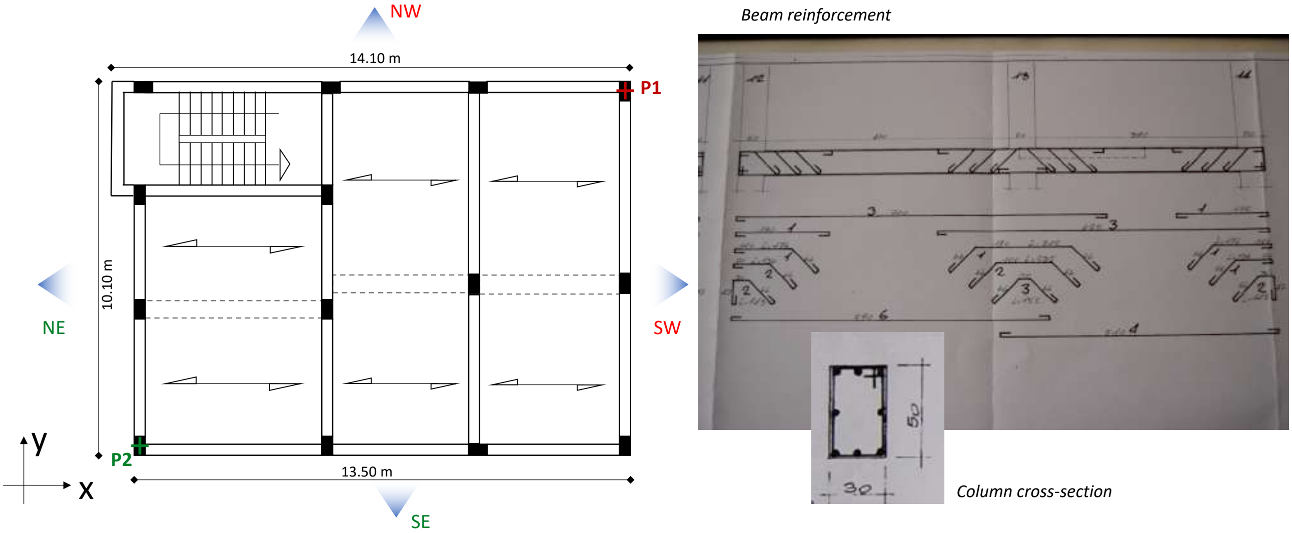


Figure 7. Structural plan and drawings of the case-study

A field survey was carried out after L'Aquila earthquake to report the damage state of the building. While no significant damage was observed for structural members, the reported pictures are principally those regarding damaged exterior infill walls. For each modelled infill wall, the graphical sketches together with the available photos allowed an estimation, based on expert judgment, of the attained Damage State (DS). As far as the criteria adopted to attribute the DS, reference has been made to the descriptions proposed for the infill damage in the EMS98 metric (Grunthal 1998) integrated by further specifications useful for the purposes of this work (see Table 4), as derived from (Del Gaudio et al. 2019, Del Gaudio et al. 2021) accounting also for the AeDES metric (Baggio et al. 2007). In particular, the final DS attributed to infill walls is graduated on three grades. More specifically, according to (Grunthal 1998), DS1 is associated with presence of light cracking in the infill panel (potentially also as detachment between the infill panel and the surrounding frame); DS2 is characterized by wider cracks with respect to DS1 and by limited plaster detachment; DS3 is characterized by failure of the panel (i.e., according to Del Gaudio et al. 2019, Del Gaudio et al. 2021), by the spalling of brick units in at least the 30% of the panel area). Note that the damage metric adopted for the assessment of Damage States in infill walls only accounts for the damage due to in-plane seismic actions. This is due to the lack, in the literature, of a consolidated damage metric also accounting for out-of-plane actions. This critical point will be further examined in section 5.2.

Some pictures and sketches of the damaged building are reported in Figure 8. Note that cracks reported in correspondence with structural members are referred to the plaster covering them, not to structural damage. For NE side, wide cracks trespassing infill walls are visible in correspondence with the staircase, and at the second storey just alongside the staircase, together with crushing of corner/bottom brick units and loss of plaster. This is consistent with the attainment of DS2. First-storey and third-storey infills alongside the staircase present quite light cracking, which is compatible with the attainment of DS1. For SW side, at the first storey, wide cracks trespassing infill walls are visible together with crushing of corner/top brick units and loss of plaster. This is consistent with the attainment of DS2. Second-storey and third-storey infills present quite light cracking, potentially associated with the detachment of the infill from the confining structural members, which is compatible with the attainment of DS1. For SE side, infills at the first storey were not modelled due to the presence of wide openings. Second-storey and third-storey infills present quite light cracking, with some loss of plaster but no crushing of brick units. This is compatible with the attainment of DS1. The condition of the central panel at the second storey may be considered “border-line” between DS1 and DS2 due to the detachment of plaster. However, the absence of visible and significant cracks made the Authors lean towards the assignment of DS1 also for this panel. For NW side, a light damage was observed. This is consistent with the attainment of DS1 or DS0.


Figure 8. Damage attributed to the exterior infill walls of the RC building

### 3.4.PRC building in San Felice Sul Panaro

The considered building is located in the municipality of "San Felice sul Panaro", as one of URM study cases. From a geomorphological and topographical point of view it is a flat area. The investigations previously carried out on soils near the site under examination revealed that the foundation soil is of type C, according to the Italian classification. The considered case study is a single-story PRC manufacturing building with masonry infills on the perimeter (Figure 9).

The building documentation is available (architectural and structural drawings, construction details, material specifications) and some non-destructive tests were also carried out in the aftermath of the earthquake to confirm the concrete strength and the reinforcing bars arrangement at the columns base. The building has a rectangular plan dimension equal to approximately 35x11 $m^2$ with a net height under the beam equal to 6.20 m. The vertical bearing structure is made up of 14 precast columns with a pocket footing foundation. The main frame of the building is made up of double-tapered girders (with a height that varies between 0.60m and 1.95m at the ridge) with a net span equal to 12 m and a portal-to-portal distance of 6 m. The secondary roof system is formed by double-T roof elements simply resting on the beams, thus relying on a friction constraint. The columns have a square cross-section of 35x35 $cm^2$ with four 14mm diameter longitudinal rebars and 5mm diameter stirrups spaced 20cm centre to centre. Furthermore, each column has a RC fork at the top in which the beam is housed to avoid overturning movements, relying, also in this case, on a frictional connection. In fact, given the period of construction (1970s), the building was designed in accordance with DM 30/5/1974 and CNR 10012/1967, which did not prescribe mechanical connections in non-seismic regions (indeed that region was not classified as seismic in those years).

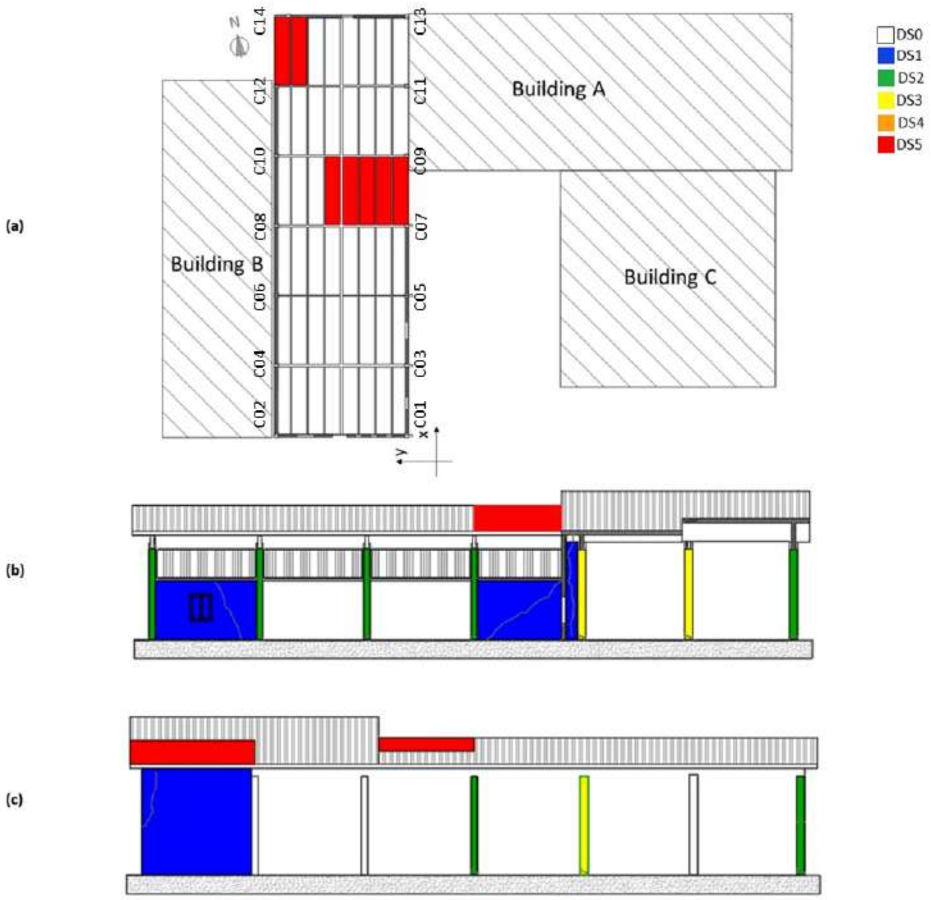


Figure 9. Post-earthquakes conditions (29/05/2012) damage states (DS): (a) plan representation; (b) Longer façade -East ; (c) Longer façade - West.

The characteristics of the materials were made available thanks to non-destructive tests carried out in the aftermath of the earthquake and from the original documentation. The material tests revealed a good quality concrete, characteristic cube strength of 35 MPa, and a Feb38k steel type, characteristic steel yield strength of 380 MPa.

As mentioned before, this building was damaged during the seismic events of May 2012. Damage was found on the structure both in the load-bearing elements and in the infills (Figure 9). Some columns (C02, C03, C05, C07 in Figure 8 experienced onset of plastic hinge development at their base and with a limited extent also in correspondence to the ribbon glazing due to the short column triggered by infill interaction. The main damage was related to the loss of support of the roof elements which caused severe damage to the building content.

## 4. Benchmarking of selected URM structures

### 4.1. Modelling and analyses

According to the adopted EF method, structural elements are idealized as nonlinear beams with lumped inelasticity and simulated by the piecewise-linear force-deformation relationship implemented in the Tremuri software (Lagomarsino et al. 2013) and formulated by (Cattari and Lagomarsino 2013b), as depicted in Figure 10a. Figure 10b-d illustrates the FE models of the three analysed buildings, where the piers and spandrels are represented in orange and green, respectively. Note that the EF model of the San Felice's-, Pizzoli's- and Visso's buildings were developed in (Cattari and Lagomarsino 2013a, DT 2013), (Degli Abbati et al. 2021), and (Brunelli et al. 2021), respectively.

The constitutive laws adopted for piers/spandrels (expressed in terms of shear-drift relation $V$- $\theta$) ensure an accurate description of the nonlinear response, also in NDAs (Cattari et al. 2018, Penna et al. 2022), as well as the definition of the attainment of specific DL (from 1 to 5) through progressive strength degradation ($\beta$) in correspondence of assigned values of $\theta$. The values assumed for $\theta$ associated with DL from 3 to 5 - and the corresponding $\beta$ - are consistent with experimental data in the literature (Beyer and Dazio 2012) (Vanin et al. 2017) (Graziotti et al. 2018) (Rezaie et al. 2020). Moreover, a hysteretic response is well reproduced through a phenomenological approach that can capture the differences among the various possible failure modes (prevalently flexural type FL, shear type SH or even mixed) and the different responses of piers and spandrels.

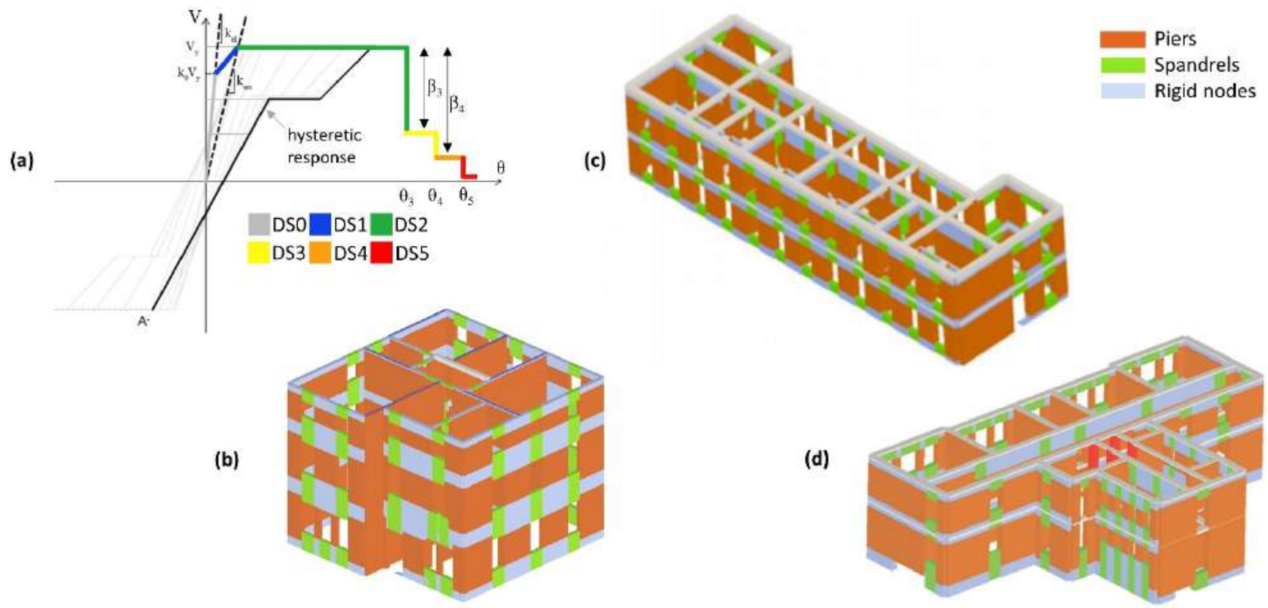


Figure 10. a) piecewise-linear force-deformation relationship implemented in the Tremuri software; b-d) EF models representing the buildings of S. Felice (b), Pizzoli (c) and Visso (d).

Regarding the criteria adopted to compute the maximum shear in panels, the shear behaviour was interpreted, for both piers and spandrels, according to the diagonal cracking failure mode proposed by (Turnšek and Sheppard 1980) (proposed as reference also in (MIT 2019), for existing masonry). Conversely, the flexural behaviour was interpreted, in the case of piers, according to the criterion proposed in (NTC, 2018) by neglecting the contribution of the masonry tensile strength, while it was differentiated, in the case of spandrels, as a function of the presence or not of a coupled tensile resistant element. More specifically, when a reinforced concrete tie beam was present at floor level (i.e. in the case of Pizzoli's- and Visso's buildings) the development of a strut mechanism was assumed and interpreted according to the criterion proposed in (NTC, 2018). Conversely, in the case of San Felice's building, the contribution of an equivalent tensile strength associated with the interlocking phenomena that could originate at the end sections of spandrels was considered according to the formulation proposed in (Cattari and Lagomarsino 2009). Strength parameters were assumed according to the masonry typology of the investigated buildings and are compatible with those proposed in (MIT, 2019) as well as consistent with some evidence from experimental results available in the literature cited above.

Table 4 and Table 5 list the main mechanical properties and the nonlinear parameters adopted in the numerical simulations.

Table 4. Mechanical parameters adopted in Tremuri for the masonry panels (*original masonry; ** masonry strengthened through mortar injections)

| Study case | | $f_m$ [MPa] | $\tau_0$ [MPa] | E [MPa] | G [MPa] |
|---|---|---|---|---|---|
| S. Felice | | 2.8 | 0.100 | 675 | 225 |
| Pizzoli | | 5.95 | 0.120 | 2262 | 754 |
| Visso | * | 4.94 | 0.096 | 2574 | 858 |
| | ** | 5.70 | 0.111 | 2701 | 991 |

Table 5. Nonlinear parameters adopted in Tremuri for masonry panels in NDA (Piers/Spandrel) for prevailing shear behavior (SH) and flexural behavior (FL). [* = defined for a prefixed value of ductility equal to 2]. Please see also Figure 10a for understanding the meaning of those parameters.

| Study case | $\theta_{E3}$ [%] | $\theta_{E4}$ [%] | $\theta_{E5}$ [%] | $\beta_{E3}$ [-] | $\beta_{E4}$ [-] |
|---|---|---|---|---|---|
| San Felice | 0.3/0.2(SH) | 0.5/0.6(SH) | 0.7/2(SH) | 0.3/0.5(SH) | 0.6/0.5(SH) |
| | 0.6/0.2(FL) | 1.0/0.6(FL) | 1.5/2.0(FL) | 1.0/0.5(FL) | 0.15/0.5(FL) |
| Pizzoli | 0.45/*(SH) | 0.7/1(SH) | 0.9/1.5(SH) | 0.6/0.7(SH) | 0.1/0.7(SH) |
| | 0.60/*(FL) | 0.8/1(FL) | 1.1/1.5(FL) | 1(FL) | 0.8/0.7(FL) |
| Visso | 0.45/* (SH) | 0.7/1.5 (SH) | 1.48/2.0(SH) | 0.4/0.3(SH) | 0.8/0.3 (SH) |
| | 0.60/* (FL) | 0.8/1.5 (FL) | 1.81/2.0(FL) | 0/0.3 (FL) | 0.15/0.3(FL) |

Figure 11a-c illustrates the response simulation of the panels tested in the experiments aiming to calibrate the parameters governing the hysteretic response of the URM elements of the San Felice’s case. In particular, for piers, two panels with different slenderness (equal to 1.35 and 2 for squat and slender piers defined in Figure 11a and Figure 11b, respectively) tested at the ISPRA laboratory (Anthoine et al. 1995) were assumed as reference. They were composed of clay brick and mortar joints and exhibited prevalent diagonal cracking and flexural crack modes, respectively. Instead, the spandrel tests of Figure 11c referred to (Beyer and Dazio 2012). These results were useful for differentiating the calibration of the parameters as a function of the prevailing failure modes and also between piers and spandrels. In the case of stone masonry, more representative of Visso’s and Pizzoli’s buildings, reference was instead made to the experimental tests described in (Magenes et al. 2010), for piers, and in (Graziotti et al. 2012), for spandrels.

Finally, it is worth specifying that, in the numerical simulations, the mechanical parameters were conventionally considered deterministic, as possible sources of uncertainties were already investigated in (Cattari and Lagomarsino 2013a, DT 2013, Degli Abbati et al. 2021, Brunelli et al. 2021) for those EF models. The interested reader may refer to (Cattari et al. 2018, Bracchi et al. 2015, and Ottonelli et al. 2021) for a more detailed discussion of this as well as the quantification of such uncertainties.

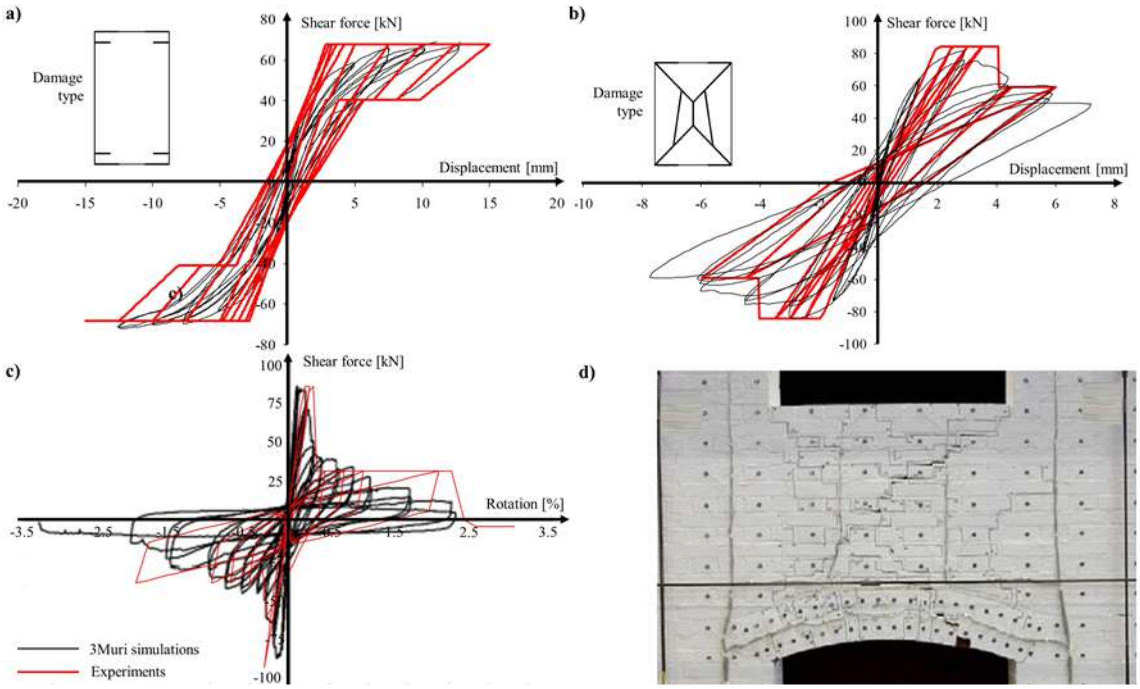


Figure 11. Calibration procedure of the mechanical parameters governing the hysteretic response of the pier elements (a, b) and spandrel element (c); in (d) is reported the damage on the spandrel observed in the experiment (Beyer and Dazio, 2012).

### 4.2. Outcomes of the applied methodology

The results of NDAs performed on the numerical models of the URM buildings are illustrated in Figure 12. In particular, the NDA curves are compared with the NSA ones. The latter analysis was useful to define the GC thresholds of the buildings corresponding to the maximum inter-story drift for which degradation of the total base shear below 50% of the maximum base shear that occurred (according to (Lagomarsino et al. 2022) and as adopted in the RINTC project). The GC thresholds are represented by the red x-markers on the NSA curves. Note that the NSAs were performed by considering both uniform load pattern distributions proportional to the mass and the first-mode shaped pattern. For the sake of clarity, only selected NSA curves are represented in Figure 12: for the San Felice's and Visso's buildings the one obtained from the first load pattern distribution while for the Pizzoli's building the one obtained from the second load pattern distribution. Indeed, the latter case showed limited nonlinear demand and, therefore, that load distribution may better represents its actual seismic structural response. Note that, for the sake of simplicity, accidental eccentricity was disregarded in the NSAs. In Figure 12, also the UPD thresholds are represented. Contrary to GC, UPD was instead defined from the damage level that occurred in the NDAs (Lagomarsino et al. 2022). In particular, the occurrence of the UPD is assumed to be attained when DL2 occurred for at least 50% of the pier elements of the considered building and/or when DL3 occurred for at least one pier element. This condition is confirmed by the graphs on the right, which show the extension of the cumulative damage (DL2 and DL3) that occurred for the piers of the investigated buildings.

Definitively, validation of the numerical simulations was performed through the identification of the effective occurrence of UPD and GC by computing the dimensionless parameter $\hat{Y}$ (Demand/Capacity ratio) as the ratio between the maximum displacement that occurred during the NDAs and the UPD/GC thresholds. It is worth noting that, the $\hat{Y}_{GC}$ refers to the maximum value computed between the negative and positive verse of the analyses. Table 6 summarizes the occurrence of both the UPD and GC for the three case studies through numerical investigation. In particular, one can see that UPD threshold was definitely exceeded for both the S. Felice's and Visso's buildings (in both the X and Y directions), whereas the Pizzoli's building attained the UPD limit only for the Y direction. These results can be confirmed by the observed DL discussed above for the three buildings.

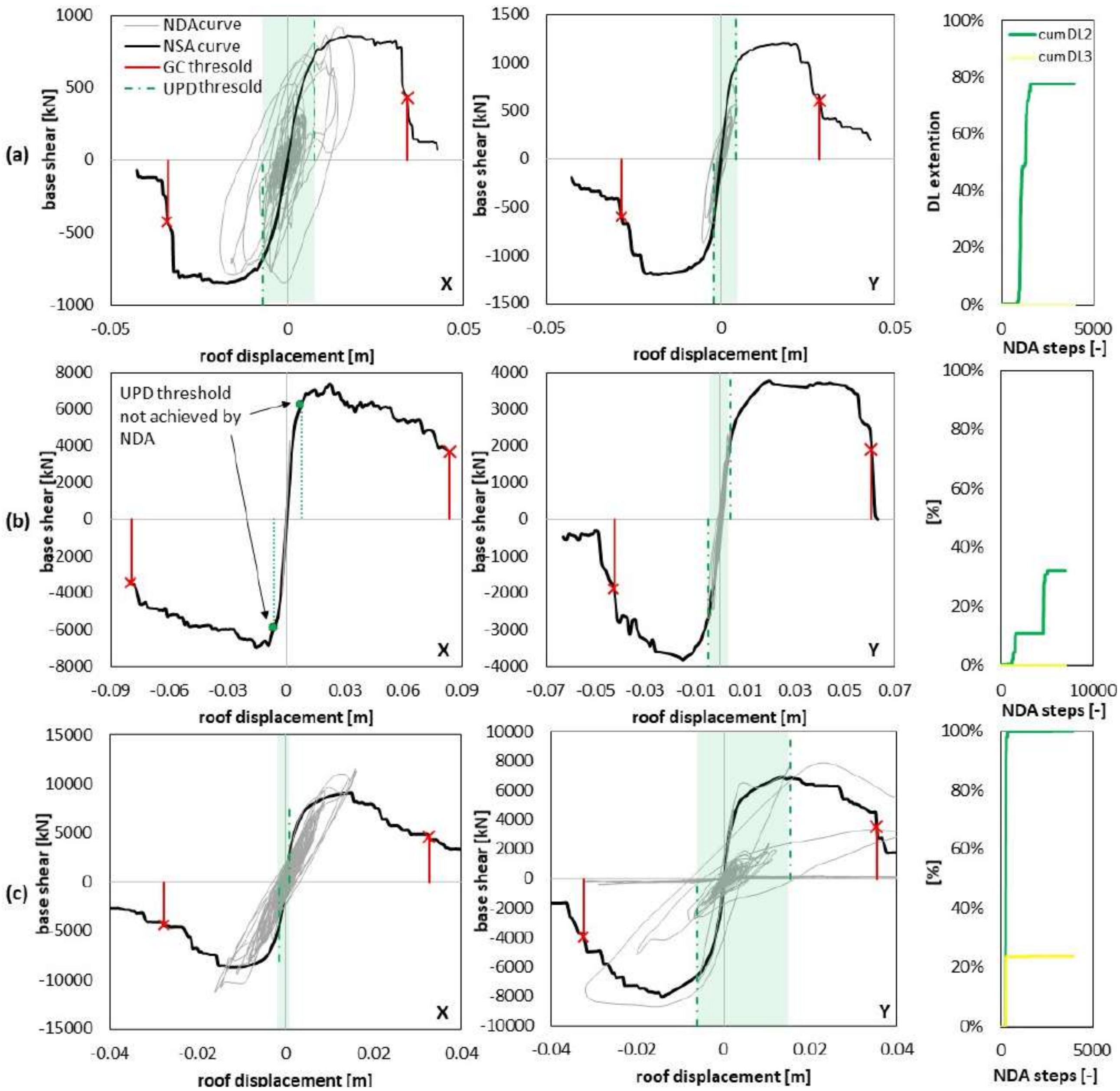


Figure 12. Comparison between NDA and NSA curves performed in X and Y directions (left and center) with indication of the UPD and GC thresholds as well as the cumulative curves of DL2 and DL3 (right) of: (a) The San Felice's case; (b) the Pizzoli's case; (c) The Visso's case.

Table 6. Verification of the occurrence of UPD and GC during NDAs

| | UPD, X | GC, X | UPD, Y | GC, Y |
|---|---|---|---|---|
| **S. Felice** | Yes ($\hat{Y}_{UPD}>1$) | No ($\hat{Y}_{GC}=0.57$) | Yes ($\hat{Y}_{UPD}>1$) | No ($\hat{Y}_{GC}=0.20$) |
| **Pizzoli** | No ($\hat{Y}_{UPD}<1$) | No ($\hat{Y}_{GC}=0.03$) | Yes ($\hat{Y}_{UPD}>1$) | No ($\hat{Y}_{GC}=0.12$) |
| **Visso** | Yes ($\hat{Y}_{UPD}>1$) | No ($\hat{Y}_{GC}=0.49$) | Yes ($\hat{Y}_{UPD}>1$) | Yes ($\hat{Y}_{GC}>1$) |

Furthermore, for all the investigated cases, the GC was attained only in the simulation of the Visso's case (Y direction). Also, this aspect is confirmed by the observed damage, as it is reasonable that the Visso's building attained its ultimate capacity, although the total collapse of the structure was not observed.

Hence, the damage level that occurred for the numerical model under NDAs is compared with that observed during the real earthquakes that struck the study case buildings. In particular, the DL at panel scale (piers and spandrels) was assigned through the attainment of the drift thresholds set in Table 5 while the DL at wall scale was assigned consistently with the method described above. Figure 13 illustrates the comparison between numerical and observed results in terms of the overall sum of weighted DL of walls (i.e. $DL_W$) differentiated between two main directions (X and Y, as introduced in Figure 4). This sum may be viewed as information on the global damage suffered by the buildings. In general, the overall damage is slightly overestimated by the numerical models particularly in the case of the San Felice's building for which the characterization of mechanical parameters was affected by higher uncertainty than the other cases (please remember that in this study the effects of uncertainties have not been examined). Moreover, the reliability of the simulation in capturing the highest vulnerability direction of the buildings (for which a higher damage level was observed) was pointed out.

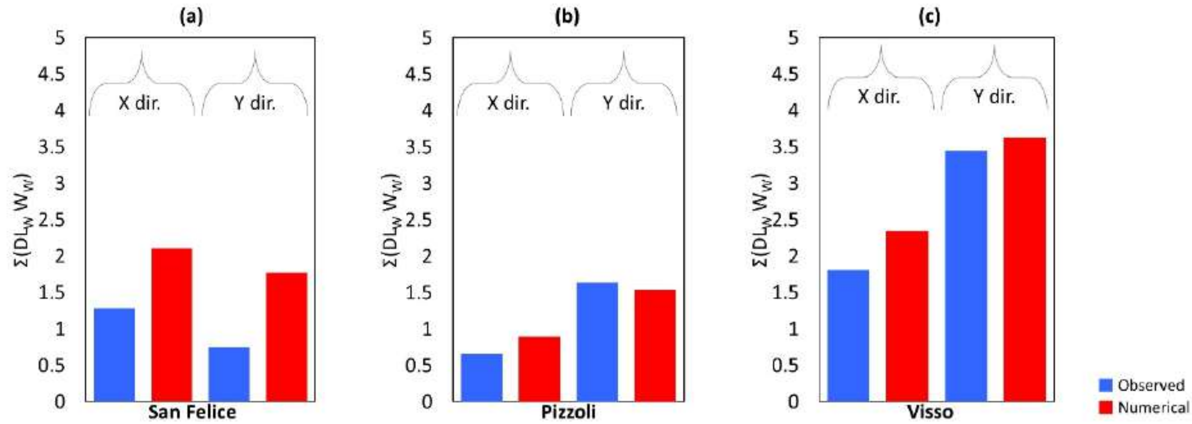


Figure 13. a-c) Observed Vs Simulated overall damage level based on the cumulative weighted damage for the four study cases.

To more accurately investigate the difference between the observed and the simulated damage and to distinguish the origin from piers or spandrels, Figure 14a-d shows the $\Delta DL_{E,SIM-OBS}$ differentiated for the piers (in orange) and spandrels (in green) belonging to each *i*-th wall of the buildings. Results show that the numerical simulations well reproduced the real damage, with values of $\Delta DL_{E,SIM\text{-}OBS}$ of about one grade for piers and slightly higher for spandrels, though the global damage level of the building is correctly reproduced. Note that, in most cases, the damage level is well captured for the structural elements belonging to walls characterized by high weight factor ($W_W$) values. For instance, the difference of 3 grades between numerical and simulated damage observed for both pier- and spandrel- elements of the wall n.15 of the San Felice's building (see Figure 4 for the localization of the wall ID) is insignificant, as the $W_W$ associated with that wall is almost null. On the contrary, the San Felice's wall characterized by the highest $W_W$ (i.e. wall n.7) has $\Delta DL_{E,SIM\text{-}OBS}$ maximum equal to 1 for pier and spandrel elements.

Despite the slight overestimation of the simulated damage, Figure 15 shows how the EF model of the San Felice's building is able to well capture the damage concentration in the spandrels at the upper level as well as the type and entity of damage that occurred in the piers; an analogous comment is valid also for the other numerical models.

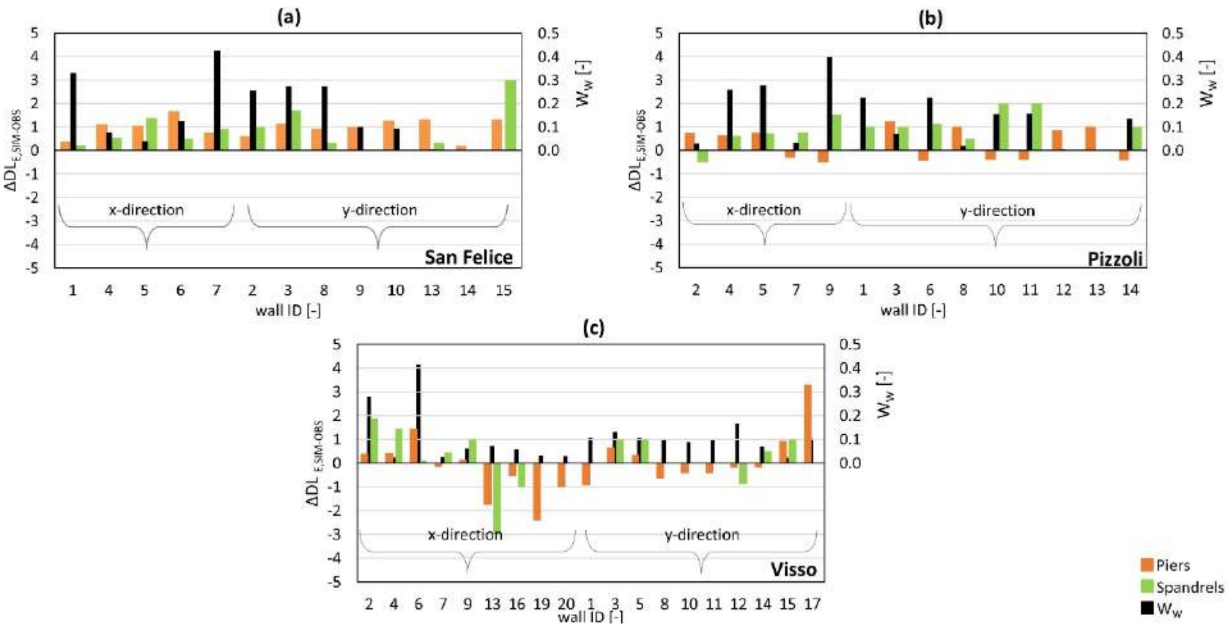


Figure 14. Differences between simulated and observed damages for all the piers and spandrels of the walls of analyzed buildings together with the indication of the wall weights ($W_W$).

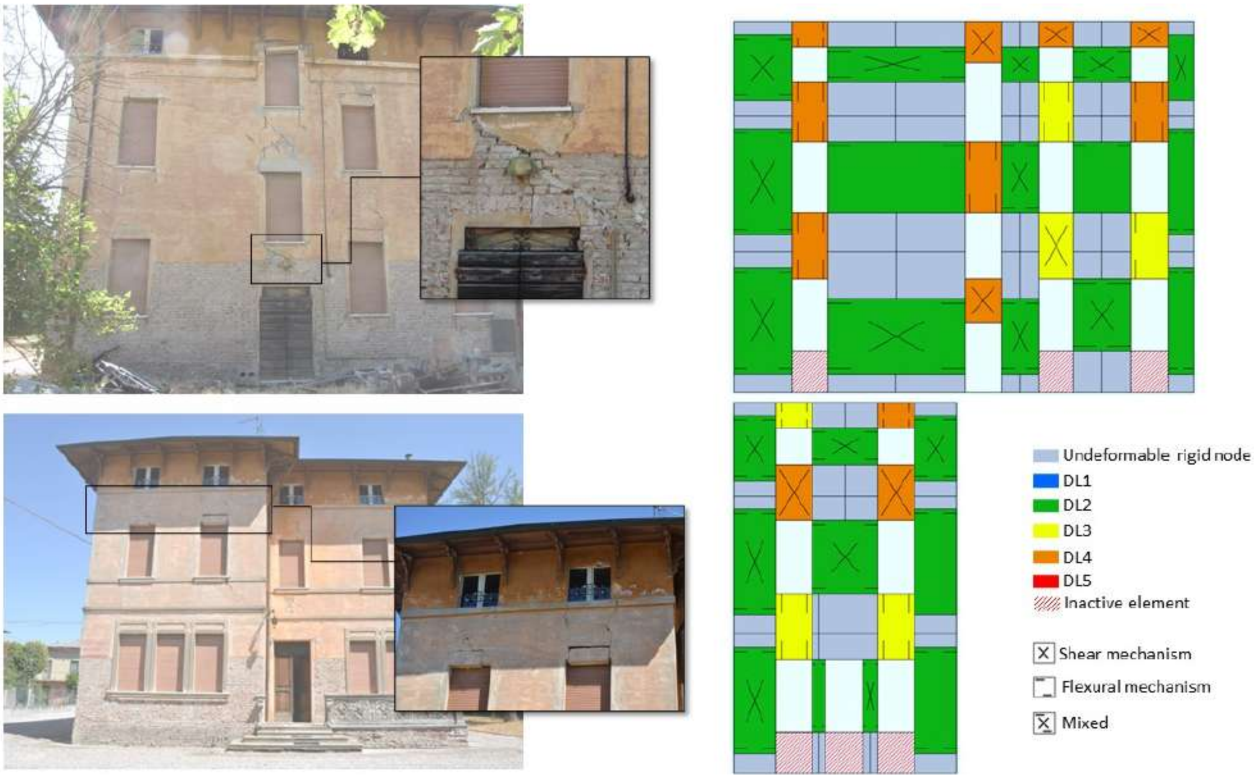


Figure 15. Comparison between the observed damage of the San Felice's case and that reproduced by numerical simulation (the original 3Muri color pattern was modified to be consistent to the colors assigned to each DL).

Finally, the reliability of the nonlinear results and, therefore, the effectiveness of the EF models in capturing the real damage state of the buildings is provided by the MI values reported in Table 7 and expressed as a function of the wall. Note that in Cattari et al. (2022), the MI has been differentiated also as a function of the structural elements (namely, walls or piers) by attributing also different weights to $MI_E$ as a function of the severity of the observed damage to better reward the models that well captured the severe or very severe DL.

Table 7. MI values computed at the wall-level for each URM buildings.

| San Felice | Pizzoli | Visso |
|---|---|---|
| 0.60 | 0.81 | 0.73 |

The lower MI value is obtained for the San Felice's building, mainly due to the higher uncertainty in both URM mechanical parameters and ground motion (that building was not monitored). In general, the MI values obtained for the URM buildings can be considered acceptable also considering the capability of the modelling approach in simulating the different damage levels that occurred in the three buildings, which are also characterized by different plan configurations. An example of sensitivity analyses aimed to exploit the use of MI to address possible uncertainties in the modelling of URM buildings is reported in Cattari et al. (2022).

## 5. Benchmarking of selected RC and PRC structures

### 5.1. Modelling and analyses

Given the purposes of this study, the nonlinear model of the case-study structure was built in OpenSees software (McKenna et al. 2000) according to the assumptions and approaches adopted for the assessment of the archetype buildings analyzed for RINTC-e project. These assumptions and approaches are briefly recalled in this section, but more details are reported in De Risi et al. (2022) and in Di Domenico et al. (2022) for RC buildings and in Bosio et al. (2021) for PRC buildings. A sketch of the modelled structures (the RC case is represented without infill walls for the sake of clarity) is reported in Figure 16.

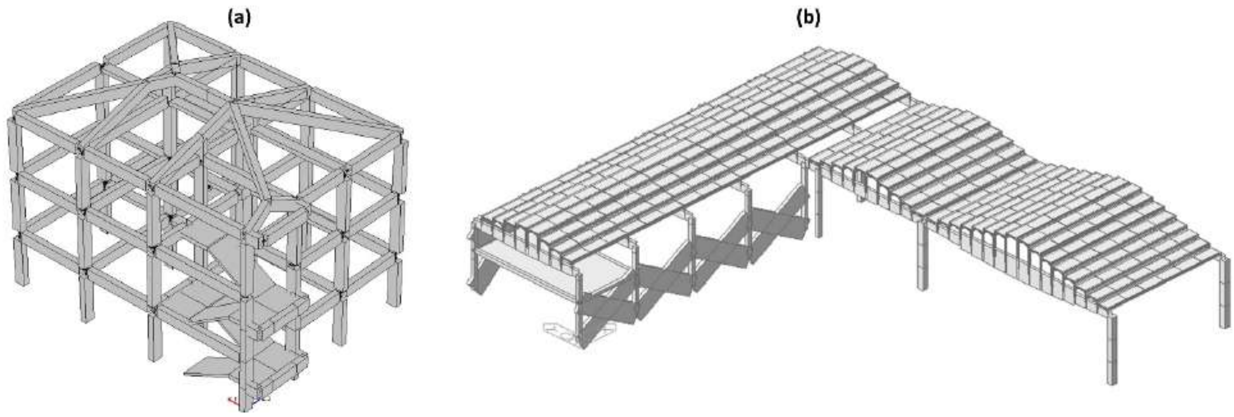


Figure 16. Reinforced concrete models: a) cast-in-place RC structure represented without infill walls; b) PRC structure

A lumped-plasticity approach is adopted to introduce nonlinearity to both structural and nonstructural elements. Since RC columns are made with plain bars, Pinching4 Material is adopted to model their nonlinear response with characteristic points of the moment-chord rotation response envelope determined for reinforced concrete columns with plain bars according to (Di Domenico et al. 2021a). These equations and rules were derived based on the experimental database collected in Verderame and Ricci (2018), constituted by 51 columns with plain rebars tested with cyclic loading. These equations are completely empirical and, so, they implicitly account, when calculating moment and deformation capacity (in terms of chord rotation), for all the phenomena that columns with plain rebars actually exhibit when subjected to cyclic lateral loading, such as bar slip.

In PRC building, columns are made with deformed bars, hence the Modified Ibarra-Medina-Krawinkler Material is adopted to model their nonlinear response with characteristic points of the moment-chord rotation response envelope determined for reinforced concrete columns with plain bars according to (Haselton et al. 2008) (which is the same modelling approach adopted for cast-in-plane RC buildings with deformed bars in RINTC-e project).

Note that the initial stiffness adopted for structural members in RC and PRC buildings is intermediate between the elastic uncracked one and the secant-to-yielding one, i.e., the secant-to-40% initial effective stiffness is adopted for structural members. Note also that in the PRC building models the roof elements and beams were modelled with elastic elements because, being simply supported with frictional connections, they are not expected to be damaged under the seismic loads.

For columns, the predicted response envelope is modified for shear-sensitive members after a pre-classification of the expected failure mode (De Risi et al. 2022). For shear-critical elements, the predicted backbone curve was modified based on the values of the lateral displacement at shear failure, $DR_s$, and of the lateral displacement at axial failure, $DR_a$. $DR_s$ and $DR_a$ were calculated based on the empirical proposal by (Aslani and Miranda 2005). No shear-critical member was detected in the case-study PRC structure.

In the RC building model, the joint panel model adopted herein is the so-called “scissors model” by (Alath and Kunnath 1995). A ZeroLength Element rotational spring is adopted to model the beam-column joint constitutive model by adopting Pinching4 Uniaxial Material assigned to ZeroLength Elements with characteristic points of the moment-rotation response envelope determined according to (De Risi et al. 2017) for exterior joints and according to (Celik and

Ellingwood 2008) for interior joints. In the PRC building model, the friction connection at the interface between the beam and the column and between the roof elements and the supporting beam was modelled by means of the "Coulomb friction" hysteresis (McKenna et al., 2000). While the mutual contact between the different structural elements (between the roof elements and between each roof element and the supporting beam) was inserted with compression only links using an "Elastic-Perfectly Plastic Gap" material (McKenna et al. 2000). Given that the case-study PRC building is part of an aggregate of similar manufacturing buildings, its numerical model also considers the potential interaction with adjacent buildings.

Exterior masonry infills are modelled by adopting equivalent concentric no-tension struts for each leaf. For masonry infill panels, material properties are assumed in order to be representative of "light" nonstructural masonry, likely present in existing RC buildings, based on the data collected in (Liberatore et al. 2018), assuming a masonry compressive strength $f_m$=2 N/mm$^2$, a masonry shear strength $\tau_{m0}$=0.4 N/mm$^2$, a basic shear strength of bed joints $\tau_0$=0.27 N/mm$^2$, and a modulus of elasticity $E_m$=1500 N/mm$^2$. As above stated, unfortunately, the real mechanical properties of masonry are not known, hence they were assumed equal to those already adopted to model the infill walls of the archetype buildings analyzed in the project. Both the in-plane and the out-of-plane response of infills was considered separately for each leaf. Regarding the in-plane response, the nonlinear behaviour was represented by means of Concrete01 Material model with characteristic points determined according to (Decanini and Fantin 1986, Decanini et al. 2014, Noh et al. 2017). The effect of openings is taken into account according to (Decanini et al. 2014). Regarding the out-of-plane response, the trilinear response envelope proposed by (Ricci et al. 2020) was adopted. However, after the attainment of peak load, a softening branch was introduced up to the attainment of zero out-of-plane resistance at an out-of-plane central displacement equal to 0.80 times the leaf thickness, similarly to the approach described in (Di Domenico et al. 2021b). The in-plane/out-of-plane interaction effects were considered, too, by adopting the modelling strategy proposed by (Ricci et al. 2018). As also done for the archetype case-study structures in (Di Domenico et al. 2022), a preliminary check was performed to assess the sensitivity of reinforced concrete members to a potential shear failure due to local interaction between infill walls and columns. It consists in the comparison between the maximum shear strength of the potential "short column" forming at the top and at the bottom of the column, due to potential local shear interaction, and an estimate of the maximum expected shear demand given by one-half the horizontal strength of infill walls plus the plastic shear of the short column. Based on this check, no potential failure due to local shear interaction was detected.

### 5.2. Outcomes of applied methodology for RC

As far as the steps of numerical analyses is concerned, first, the nonlinear model of the bare frame was built; second, gravity loads were applied; third, infill walls were introduced in the structural model; fourth, eigen analysis (Table 8) was performed; finally, nonlinear time-history analyses were performed.

According to the eigen analysis, the first vibration mode ($T_1 = T_{1,Y}$=0.345 s) is principally associated with a translation of the structure along the transverse (Y) direction, the one in which the structure is framed. It results in a more deformable with respect to the longitudinal (X) one for both the presence of infilled walls and the "bracing" effect of the staircase members along the longitudinal direction. The second vibration mode ($T_2$=$T_{1,X}$=0.293 s) is principally associated with a translation along the longitudinal direction of the structure plus a non-negligible torsion around the vertical axis.

Table 8. Selection of modal properties of the case-study structure

| Vibration Mode | 1 | 2 |
|---|---|---|
| Direction with maximum participating mass ratio | Transverse (Y) | Longitudinal (X) |
| Participating mass ratio | 84% | 54% |
| Period T | 0.345 s | 0.293 s |
| $S_a$(T)-AQK | 0.487 g | 0.383 g |
| $S_a$(T)-MONITOR | 0.380 g | 0.672 g |

From the results reported in Table 8, AQK record is expected to produce higher demand in the transverse direction than MONITOR record; the contrary is expected to occur in the longitudinal direction.

Nonlinear time-history analyses were performed by adopting mass- and initial stiffness-proportional Rayleigh damping model. Damping coefficients were calculated by assigning a damping ratio equal to 5% to one-half the first vibration frequency and to the fifth vibration frequency of the structure, consistently with the approach adopted for the multi-stripe analysis of the archetype buildings carried out for the project.

Given the aims of this study, the results of nonlinear time-history analyses performed by adopting both AQK and MONITOR records are reported in Table 9 in terms of maximum absolute interstorey-drift ratio (IDR) demand. The $IDR_{max}$ values were determined by considering the lateral displacement in longitudinal and transverse directions of control points P1 and P2. In addition, the $\Delta_{TOP,TH}$ values were determined by considering the lateral displacement in both longitudinal and transverse directions of the roof centroid.

Table 9. Results of nonlinear time-history analyses in terms of maximum IDR demand

| Direction | | Side | Storey | AQK | MONITOR | Average |
|---|---|---|---|---|---|---|
| longitudinal | $IDR_{max}$ [%] | NW | 1st | 0.14 | 0.19 | 0.17 |
| | | | 2nd | 0.17 | 0.22 | 0.20 |
| | | | 3rd | 0.15 | 0.17 | 0.16 |
| | | SE | 1st | 0.31 | 0.29 | 0.30 |
| | | | 2nd | 0.36 | 0.36 | 0.36 |
| | | | 3rd | 0.19 | 0.22 | 0.21 |
| | $\Delta_{TOP,TH}$ [mm] | | | 18 | 20 | 19 |
| transverse | $IDR_{max}$ [%] | NE | 1st | 0.31 | 0.25 | 0.28 |
| | | | 2nd | 0.39 | 0.32 | 0.36 |
| | | | 3rd | 0.26 | 0.19 | 0.23 |
| | | NE (staircase*) | 1st | 0.18 | 0.15 | 0.17 |
| | | | 2nd | 0.42 | 0.36 | 0.39 |
| | | | 3rd | 0.29 | 0.22 | 0.26 |
| | | SW | 1st | 0.42 | 0.34 | 0.38 |
| | | | 2nd | 0.52 | 0.39 | 0.46 |
| | | | 3rd | 0.30 | 0.24 | 0.27 |
| | $\Delta_{TOP,TH}$ [mm] | | | 30 | 24 | 27 |

(*): for infill walls enclosing the staircase, specific values of $IDR_{max}$ were calculated considering the presence of quarter landings.

As expected, maximum IDR demands were observed for the building sides farther from the staircase (SW and SE). The significant difference between maximum IDR demands for NW/SW and SE/NE sides highlights the presence of a torsional response of the structure. In addition, despite being a low-rise building, the maximum IDR demand is always registered at the second storey. This highlights the importance of higher modes in the structural response of the case-study building. This is most likely due to the eccentricity of stiffness centroid with respect to mass centroid produced by the eccentricity of the staircase position in the structural plan as well as to the irregular distribution of solid/opened infill walls in the building plan and elevation. Finally, AQK record produces higher IDR and top displacement demand in the transverse direction, while MONITOR record produces generally higher IDR and top displacement demand in the longitudinal direction, as expected by comparing modal analysis results with the response spectra of the records.

According to (Di Domenico et al. 2022), for infilled reinforced concrete moment-resisting frames, a multi-criteria approach is adopted to identify the attainment of UPD Limit State. Namely, UPD Limit State is attained when the first of the four following conditions occurs:

- the top displacement demand attains the displacement at the attainment of 95% of the maximum base shear (in the ascending branch of the pushover curve);
- at least one-half of the infill walls of the building has attained a shear demand equal to the expected horizontal strength (i.e., has attained DS2);
- at least one infill wall has attained a horizontal displacement demand corresponding to a 50% degradation of the infill horizontal strength capacity (i.e., has attained DS3);
- OOP collapse of an infill wall (assessed from time-history analyses).

Pushover analyses were performed to evaluate the displacement capacity at UPD Limit State and at GC Limit State. More specifically, pushover analyses were performed by pushing the structure along the longitudinal and transverse directions, both in the positive and in the negative direction, by applying two different lateral load patterns: a first-mode shaped pattern and a uniform pattern. A total of 8 pushover curves were derived. According to the pushover analyses performed, the top displacement at the attainment of UPD Limit State, which is always due to the occurrence of condition i) before condition ii) and iii), ranges from 38 to 57 mm for the longitudinal direction and from 56 to 78 mm for the transverse direction of the case-study building. Results are shown in Figure 17 comparing the roof displacement – base shear time-history response with the corresponding pushover curve. Only for representation purposes, the shown pushover curves are related to the modal lateral force pattern: in fact, it is observed that during the time-history analyses the structure remains in the elastic stage and experiences only limited nonlinear demand. Hence, it is expected that the response to a modal lateral force equivalent pattern better represents the response of the structure in the range of interest of the displacement demand. Note also that, differently from the methodology adopted for masonry buildings, the check for Damage Levels exceeded by masonry infills is performed only based on pushover analysis. For this reason, the extension of the cumulative damage as a function of the time step is not reported in Figure 17.

According to the time-history results shown in section 5.3, no out-of-plane collapse of an infill was registered (i.e., condition iv) was not attained); the reference top displacement demand for the case-study structure is 19 mm in the longitudinal direction and 27 mm in the transverse direction. Both displacement values can be found in the ascending branch of the pushover curves. So, it can be concluded that neither UPD nor GC Limit States were attained based on the time-history analyses carried-out. In addition, the fact that, based on the time-history analyses, UPD Limit State is not expected to be attained due to conditions ii) and iii) is also confirmed based on the discussion reported in the following, since according to the fragility curves proposed by (Del Gaudio et al. 2021), no infill wall is expected to attain DS3, while only 11 infills out of 26 (i.e., less than 50% of the modelled infill walls) are expected to attain DS2.

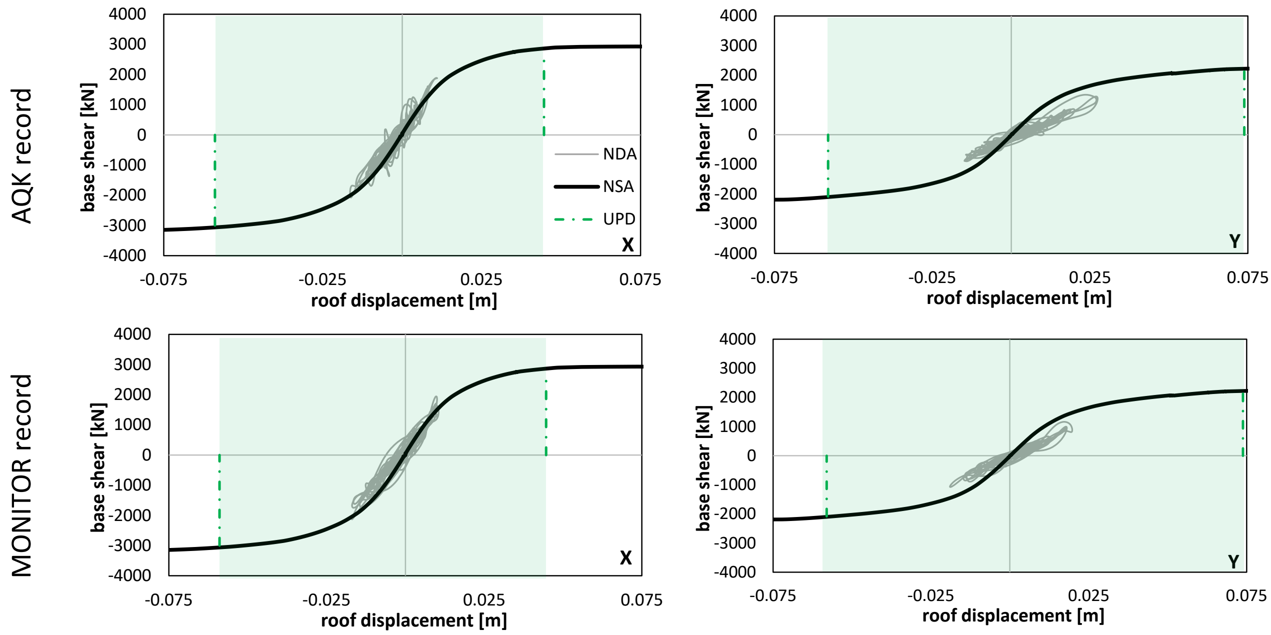


Figure 17. Pushover curves compared with the time-history response of the RC case-study structure.

All the above is consistent with the evidence of the field survey. As shown in section 5.1, based on field survey and on the visual assignment of DS to the exterior infill walls of the case-study structure, it can be concluded that neither condition ii) nor condition iii) and iv) were attained. So, UPD Limit State could have been attained only due to condition i), which corresponds, as stated in *(*Di Domenico et al. 2022*)*, to the onset of a significant lateral stiffness degradation for the structure. Unfortunately, it is not possible to assess, from field survey, the attainment of condition i), which is strictly related to the response of the entire structure. So, at least regarding conditions ii), iii) and iv) it can be assumed that the real case-study building did not attain UPD Limit State due to L'Aquila earthquake. Of course, GC Limit State was not attained since it is associated with the real collapse of the structure, which did not occur. In summary, the criteria assumed for infilled reinforced concrete buildings for the assessment of UPD and GC Limit States within RINTC-e project can be deemed acceptable as they were confirmed by the results of the benchmark analysis.

To check the efficiency of the adopted modelling strategy, the MI is calculated for both structural and non-structural members.

Regarding structural members, Criterion 1 in Table 2 is adopted for calculation of MI for each structural element. As shown in section 3.3, no significant damage is visible for structural members.

This is consistent with the assignment of DS0 to all structural members as "observed" damage state. For the assessment of the "simulated" damage level, the proposal by Del Gaudio et al. (2018) is adopted. According to this metric, a structural member is in DS0 only if it has not cracked; it is in DS1 if it has cracked but not yielded; it is in DS2 or more after yielding. According to the numerical analyses performed, all columns have cracked (hence, they have entered DS1 and have MI equal to 0.5); first- and second-storey beams have cracked (hence, they have entered DS1 and have MI equal to 0.5); third-storey and roof beams have not cracked (hence, they are in DS0 and have MI equal to 1). The average value of the MI is 0.64. This value may appear quite low. However, it should be noted that the observed DS0 for columns and part of the beams may be also due to hairline cracks formed during the earthquake (which would be consistent with the attainment of DS1 based on maximum IDR/chord rotation demand during structural analyses) and no more visible at the end of seismic excitation. Of course, some modelling assumptions may also have influenced this outcome, above all the fact that structural members were modelled by adopting an effective stiffness (thus underestimating the actual initial stiffness of uncracked members). That being said, it could be concluded that the numerical model estimates that structural members are in the range between DS0 and DS1 when the seismic input is at its maximum intensity, which is consistent with the "residual" DS0 observed for the structural members after the earthquake.

Regarding exterior infill walls, Criterion 3 in Table 2 is adopted to compute MI for each panel. First, note that during NDAs, none of the infill walls exhibited an OOP collapse, consistently with field evidence. In addition, the OOP displacement demand on infill walls deriving from analyses is limited, namely lower than the peak load displacement. Based on various experimental tests performed on infill walls similar to those present in the case-study structure (e.g., Ricci et al. 2018b, De Risi et al. 2019, Di Domenico et al. 2021d), the OOP damage effects are significantly visible only when the OOP peak load displacement of the infill wall is overcome. In other words, no significant damage due to OOP actions is expected for the infill walls of the case-study structure, thus justifying the use of a damage metric that does not consider the effects of OOP actions.

Based on the fragility curves proposed in (Del Gaudio et al. 2019, Del Gaudio et al. 2021) (see Section 2.1), and on the average IDR demand (between the AQK and MONITOR records) observed during the NDAs, the probability of observing a certain DS for each infill wall was calculated, as shown in section 2.1 as a function of the distance between the fragility curves associated with the three DLs. In particular, in Figure 18, the probability of observing a certain DS is compared with the DS assigned based on the observed damage. The latter is reported as a vertical light blue line.

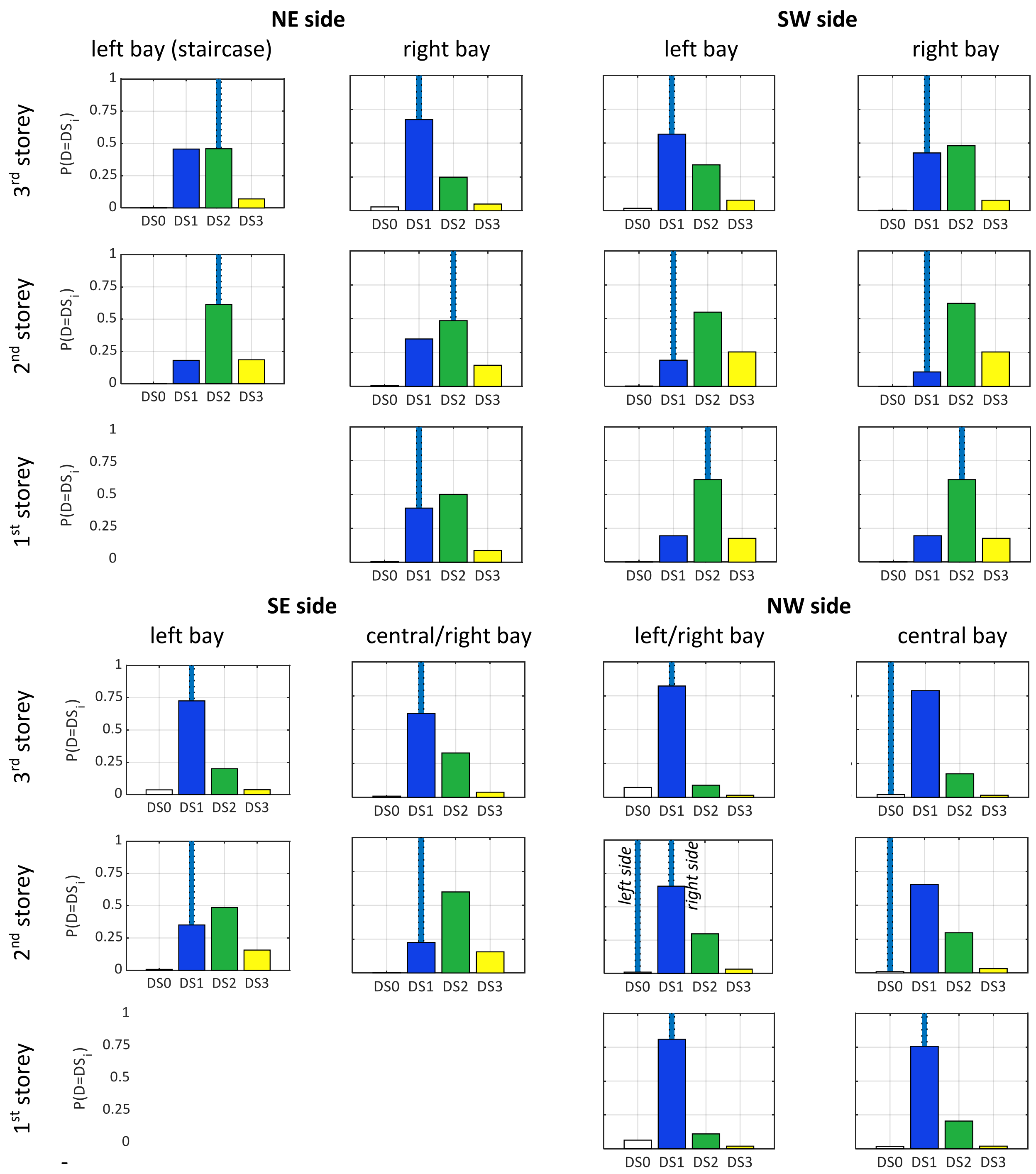

Figure 18. Comparison of the observed DS (light blue bar) with the probability distribution of observing each DS.

The effectiveness of the numerical analyses is calculated as the ratio between the sum of all $MI_j$ values and the number of the modelled infill walls, equal to 26. The estimated efficiency of the model is 0.7 (roughly equal for both directions) and, thus, generally satisfactory. In general, the error consists of an expected DS more severe than the real one. This may be due to different uncertainty sources as well as for the fact that interior partitions are not modelled, and their stiffness contribution may be not negligible at low level of the seismic demand. However, this can be considered an acceptable simplification within a collapse risk analysis, which is the core topic of RINTC-e project.

### 5.3. Outcomes of applied methodology for PRC

To evaluate the effects of the modeling choices, three models were defined with an increased level of interaction complexity (see Table 10).

Table 10. Finite element models considered for the PRC structure.

| **Model id** | **Infill Panels** | **Mutual contact between roof elements** |
|---|---|---|
| PRC01 | No | No |
| PRC02 | Yes | No |
| PRC03 | Yes | Yes |

Figure 19a shows the results obtained in terms of the number of roof elements as a function of the relative displacement demand, $\Delta$, in the beam-roof element connections. The PRC01 and PRC02 models significantly overestimate the number of fallen roof elements (i.e. with a relative displacement greater than 8 cm, corresponding to the bearing length). The PRC03 model better captures the actual distribution of fallen roof elements, highlighting the importance of including the mutual interactions between adjacent elements in the analysis. An additional sensitivity analysis was performed considering PRC03 as the reference model to investigate the influence of the aforementioned parameters: column initial stiffness scale factor ($\beta$) equal to 50% and 100%; friction coefficient ($\mu$) equal to 0.5 (i.e. concrete to concrete) and 0.13 (i.e. concrete to neoprene); damping ratio ($\xi$) equal to 1%, 3%, and 5%. One parameter at a time with respect to the reference parameters has been changed. Figure 19b shows the results obtained in terms of relative displacements of the friction connections of the roof elements for such sensitivity analysis. The results show that, considering the gross stiffness of the columns, a 10% increase in the number of fallen roof elements (i.e. $\Delta > 8$cm) is obtained. A reduction of the coefficient of friction ($\mu = 0.13$) and of the damping value ( $\xi = 3\%$) leads to a 8% and 6% increase of the fallen elements, respectively. Looking at the effectively fallen elements, these results suggest that the optimal model has the following analysis parameters: a scale factor of the initial stiffness of the columns $\beta = 50\%$, a coefficient of friction $\mu = 0.5$, and a damping ratio $\xi = 5\%$.

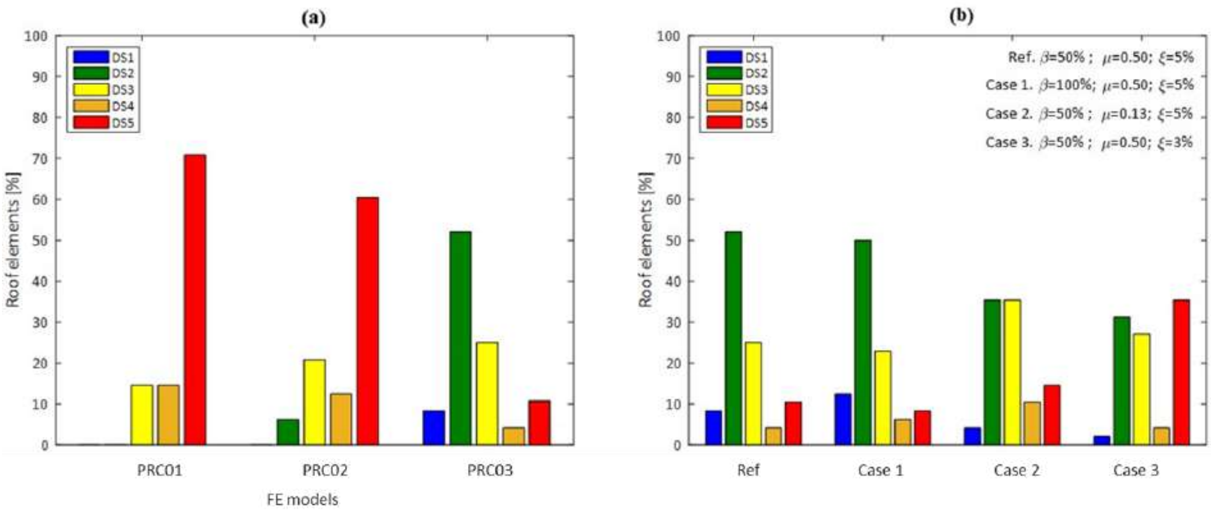


Figure 19. Number of roof elements (expressed as a percentage of the total number) as a function of the relative displacement demand: (a) considered models (PRC01, PRC02, PRC03); (b)

sensitivity analysis on the parameters for PRC03. Note: DS1 0 ≤Δ<1cm; DS2 1cm≤Δ<3cm; DS3: 3cm≤Δ<6cm; DS4 6cm≤Δ<8cm; DS5 Δ>8cm.

Figure 20 shows the result of the evaluation of the loss of support of the roof elements considering a support value of 8 cm. Comparing the numerical results with the state of damage observed after the

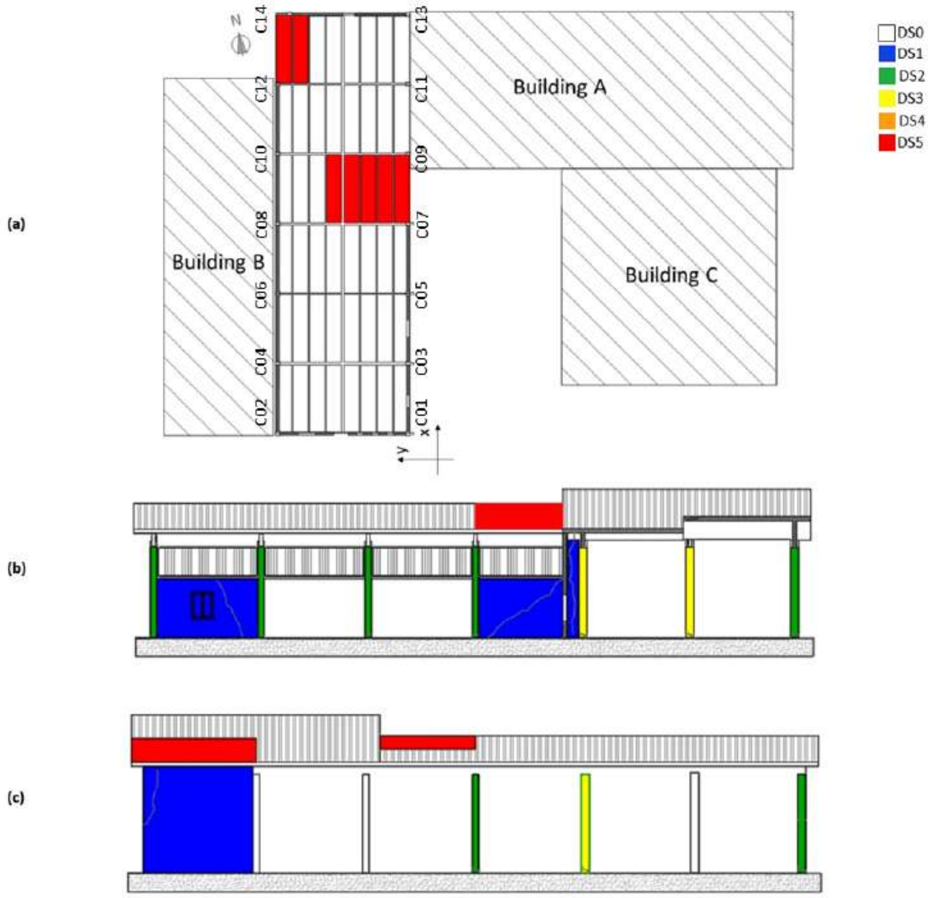


earthquake (Figure 9Figure 9), it is possible to state that the considered modelling technique allows to capture the regions of the roof where the loss of support of the roof elements has that occurred with a good accuracy.

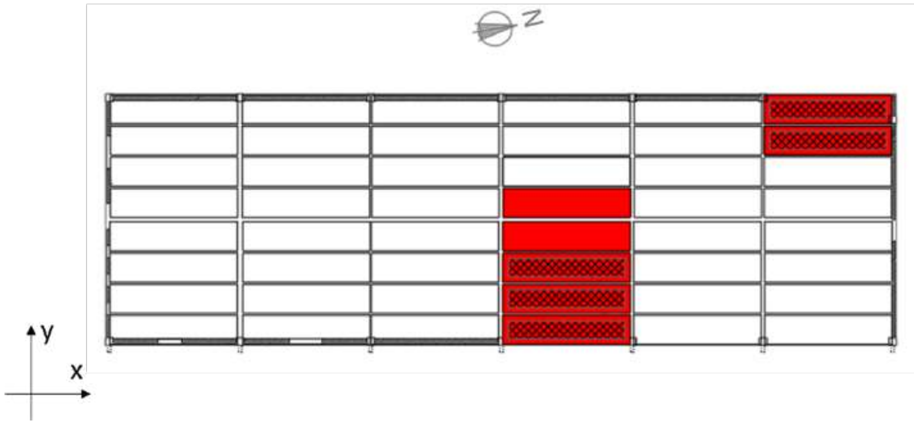


Figure 20. Results of the time history analysis of the final model. The red areas represent the actually fallen roof elements, while the hatched areas represent the roof elements of the finite element model with a relative displacement demand greater than 8 cm (i.e. eventually fallen).

The efficiency of the model is evaluated herein with the MI parameter. As shown in Figure 20, the non-linear model captured the collapse (DS5) of 5 roofing elements; for these elements $MI_E$ is equal to 1. For the other two elements supposed to be fallen, the relative displacement was ranging from 6 cm and 8 cm leading to DS4; for these elements $MI_E$=0.5. Unfortunately, the MI is not directly determinable for all the roof elements as it was not possible to detect the damage states of the connections in the not-fallen roof elements; although, it can be reasonably assumed that the not-fallen elements suffered a low level of damage (DS1, DS2) as a replacement of such elements was not mandatory. In this case (i.e. with $n_E$=48), the estimated efficiency of the model MI was equal to 0.98, whereas by considering only the fallen elements (i.e. with $n_E$=7), MI was equal to 0.86.

Another interesting point is the reasonable match between the numerical results and the actual onset of flexure cracking in the short column in the correspondence to the ribbon glaze (Figure 21 - top) and at the onset of plastic hinge development at the column base (Figure 21- bottom). Figure 22 reports some representative results for the infill walls. An approach similar to that described for the roof elements allows estimating an  efficiency of the model equal to 0.85 as regards the damage on the columns. For the infill panels, not enough information is available on the damage that occurred during the earthquake.

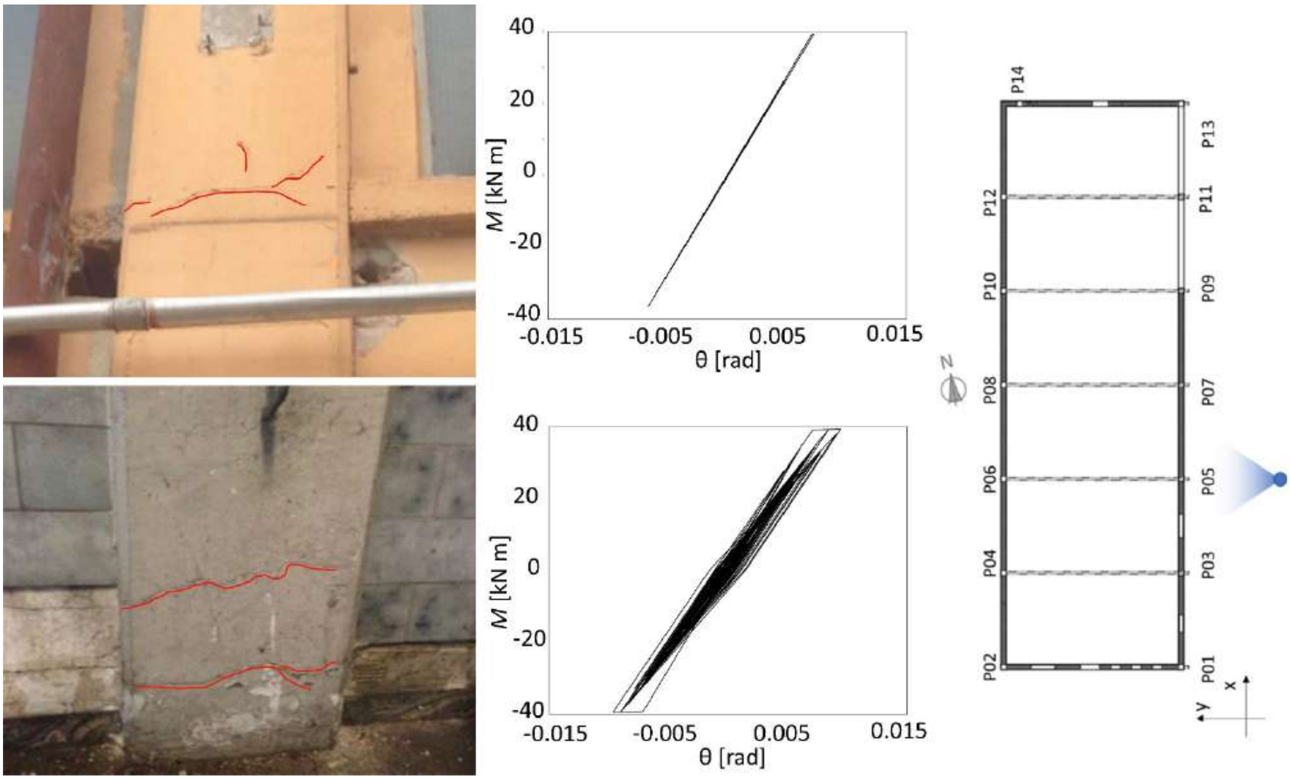


Figure 21. Comparison between the post-earthquake damage state and the numerical results for the column P05. Top: onset of flexure cracking at the short column in correspondence to the ribbon glaze. Bottom: plastic hinge at the base

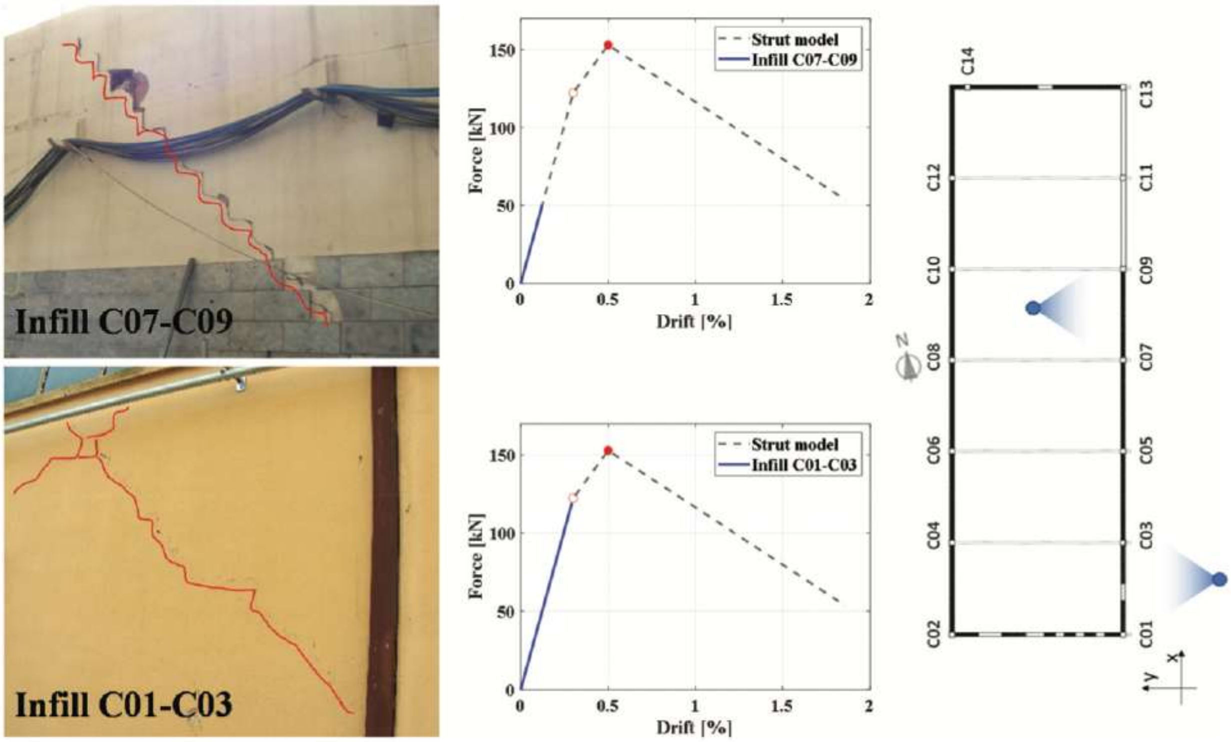


Figure 22. Comparison between the post-earthquake damage state and the numerical results for the infill walls

For PRC industrial structures, the UPD criterion is generally based on the occurrence of one of the following conditions: for infill walls the failure criterion is the same as RC buildings; in the case of cladding panels, the failure criterion is the collapse of the connections; for friction-based elements the failure criterion is the achievement of a relative displacement greater than 10% of the available seating. As for the global collapse (GC), this occurs when one of the columns reaches the chord rotation capacity (lack of rigid diaphragm assumption), when a dowel connection fails or when an element falls down from its seating.

Static nonlinear analyses (NSA) of the building were carried out separately in the X and Y directions considering a force distribution proportional to the main mode shape in each direction, respectively. Figure 23 presents a comparison between the results of the nonlinear dynamic (NDA) and static analyses considering the X direction; indeed, such direction is the one associated with the loss of seating of the roof elements (i.e. the PRC benchmark goal). This comparison is only indicative as the NSA curves do not allow to capture the actual capacity of the considered case study, in fact, the analysis ends when reaching the loss of support of one of the friction-based elements.

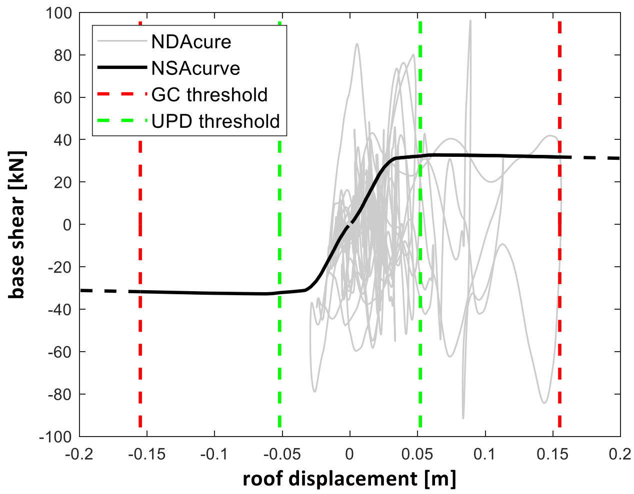


Figure 23. Comparison between NDA and NSA curves performed in the X direction.

As can be seen in Figure 19 (PRC03 – reference case), more than 50% of the roof elements are found in the DS2 which can be considered as a low damage state; from Figure 20 it appears that 5 of the 48 roof elements are in the DS5. These results further highlight that both the UPD and GC limit states considered were achieved with the time history analysis as represented in Figure 23. This is consistent with what observed in the field survey.

## 6. Conclusions

The present work investigated the effectiveness of modelling approaches and the consistency of the criteria defined in the RINTC research project for both the Global Collapse (GC) and Usability-Preventing Damage (UPD) limit states of different structural typologies belonging to the existing Italian building stock (i.e. unreinforced masonry (URM), precast reinforced concrete (PRC) and infilled reinforced concrete (RC)).

For the model validation purpose, an approach consistent across the various structural typologies but, at the same time, able to account for their specific peculiarities was conceived by the definition of a Matching Index (MI). MI consists of a value ranging from 0 to 1 that is addressed to quantify in a synthetic way the similarity level between the observed and simulated damage state. Values of MI around or higher than 0.6 confirm a good reliability and effectiveness of the developed numerical models as well as the reliability of the main outcomes. It is worth noting that the highest MI values (from 0.86 to 0.98) was obtained for the PRC building, which was subject to a sensitivity analysis. Indeed, this can be useful for investigating the role of various uncertainties involved in the modelling process and addressing the most reliable mechanical parameter values. However, also in the cases of RC and URM buildings, for which the numerical models were developed prior to the method's conception (and not with the aim of achieving the maximum MI for them), the results are satisfactory. In particular, the MI ranges from 0.63 (referring to the structural elements) to 0.70 (focusing to the infills), for the RC building, and from 0.60 to 0.81, for the URM buildings. Among these latter ones, the lowest value refers to the S.Felice's building, which was the only case for which data of dynamic identification was not available and, therefore, did not benefit from the initial calibration, at least for the pseudo-elastic phase (e.g. stiffness of both diaphragms or masonry) although additional uncertainties arise in the nonlinear phase.

Definitively, those results are in line with the expected results, according also to the trend of all results obtained within the RINTC-e project and summarized in Iervolino et al. (2021), where URM structures are associated with the highest dispersion on results.

The results showed that the definition of selected performance levels are consistent with the evidence of the field survey. Indeed, GC thresholds were numerically achieved on the 3D models representative of the investigated buildings only when severe damage was also observed in the real structures, whereas UPD limit was actually attained in the numerical simulations of buildings characterized by slight/medium damage states.

The relevance of the present work is therefore reflected in the definition of a general method applicable to different structural typologies although the large amount of accurate information needed to apply the presented methodology may represent a limitation. Future studies will be addressed on the application of the proposed approach to other study cases. For URM structures, one could investigate also real buildings that experienced not negligible out-of-plane failures during past earthquakes. Regarding RC structures, ongoing research is focused on benchmarking of modelling strategies for structural members against the results of monitored full-scale buildings tested on shaking-tables; in addition, future research could be dedicated to a more refined benchmarking of modelling strategies for infill walls, potentially also accounting for the contribution of interior partitions. For the PRC buildings, interesting aspects are related to the benchmarking of the performance of other structural systems, such as in the case of failure of RC forks at the top of the columns or in the case of damage and failure of the connections of heavy PRC cladding panels.


## ACKNOWLEDGMENTS

The study presented in this article was developed within the activities of the ReLUIS-DPC 2019–2021 research programs, funded by the Presidenza del Consiglio dei Ministri—Dipartimento della Protezione Civile (DPC). Note that the opinions and conclusions presented by the authors do not necessarily reflect those of the funding entity. The contribution of prof. G. Castellazzi in gathering the information about the precast building case study is greatly acknowledged.

## DECLARATION OF INTEREST STATEMENT

The Authors declare that they have no conflict of interest.

## REFERENCES


Alath S., S.K. Kunnath. Modelling inelastic shear deformations in RC beam–column joints. 10th Conference in Engineering Mechanics, Boulder, Colorado, USA, May 21–24, 1995.

Angiolilli, M., Pathirage, M., Gregori, A., Cusatis, G. (2021a). Lattice discrete particle model for the simulation of irregular stone masonry. Journal of Structural Engineering, 147(9), 04021123.

Angiolilli, M., Lagomarsino, S., Cattari, S., Degli Abbati, S. (2021b). Seismic fragility assessment of existing masonry buildings in aggregate. Engineering Structures, 247, 113218.

Anthoine, A., Magonette, G., Magenes, G. (1995). Shear-compression testing and analysis of brick masonry walls. Proc. 10th European Conference on Earthquake Engineering.

Aslani H., E. Miranda. Probabilistic earthquake loss estimation and loss disaggregation in buildings. Report No. 157. The John A. Blume Earthquake Engineering Center, Department of Civil and Environmental Engineering, Stanford University, Stanford, CA, USA, 2005.

Augenti, N., Parisi, F. (2010). Learning from construction failures due to the 2009 L'Aquila, Italy, earthquake. Journal of Performance of Constructed Facilities, 24(6), 536-555.

Baggio, C., Bernardini, A., Colozza, R., Coppari, S, Corazza L, Della Bella M, Di Pasquale G, Dolce M, Goretti A, Martinelli A, Orsini G, Papa F, Zuccaro G (2007) Field manual for post-earthquake damage and safety assessment and short term countermeasures (Pinto A, Taucer F eds), Translation from Italian: Goretti A, Rota M, JRC Scientific and technical reports, EUR 22868 EN-2007.

Bazant, Z. P., Planas, J. (1997). Fracture and size effect in concrete and other quasibrittle materials (Vol. 16). CRC press.

Belleri, A., Brunesi, E., Nascimbene, R., Pagani, M., Riva, P. (2015a). Seismic performance of precast industrial facilities following major earthquakes in the Italian territory. Journal of Performance of Constructed Facilities, 29(5). doi: 10.1061/(ASCE)CF.1943-5509.0000617

Belleri, A., Torquati, M., Riva, P., Nascimbene, R. (2015b). Vulnerability assessment and retrofit solutions of precast industrial structures. Earthquakes and Structures, 8(3), 801–820. doi: 10.12989/eas.2015.8.3.801

Beyer, K., Dazio, A. (2012). Quasi-static cyclic tests on masonry spandrels. Earthquake Spectra, 907-929.

Bosio, M., Di Salvatore, C., Bellotti, D., Capacci, L., Belleri, A., Piccolo, V., Cavalieri, F., Dal Lago, B., Riva, P., Magliulo, G., Nascimbene, R., Biondini, F. (2021). Modelling and seismic response analysis of non-residential single-storey existing precast buildings in Italy. Submitted for possible publication in the Journal of Earthquake Engineering

Bournas, D.A., Negro, P., Taucer, F.F. (2014). Performance of industrial buildings during the Emilia earthquakes in North-ern Italy and recommendations for their strengthening. Bulletin of Earthquake Engineering, 12(5), 2383–2404. doi: 10.1007/s10518-013-9466-z

Bracchi, S., Rota, M., Penna, A., Magenes, G. (2015). Consideration of modelling uncertainties in the seismic assessment of masonry buildings by equivalent-frame approach, Bullettin of Earthquake Engineering, 13(11), 3423-3448.

Braga F, Manfredi V, Masi A et al. Performance of non-structural elements in RC buildings during the L'Aquila, 2009 earthquake. Bulletin of Earthquake Engineering 2011;9.1:307-324. DOI:10.1007/s10518-010-9205-7

Bressanelli ME, Bellotti D, Belleri A, Cavalieri F, Riva P, Nascimbene R. (2021). Influence of Modelling Assumptions on the Seismic Risk of Industrial Precast Concrete Structures. Front. Built Environ. 7:629956. doi: 10.3389/fbuil.2021.629956

Brunelli, A., De Silva, F., Piro, A., Parisi, F., Sica, S., Silvestri, F., Cattari, S. (2021). Numerical simulation of the seismic response and soil–structure interaction for a monitored masonry school building damaged by the 2016 Central Italy earthquake. Bulletin of Earthquake Engineering, 19(2),1181-1211.

Casotto, C., V. Silva, H. Crowley, R. Nascimbene, and R. Pinho. 2015. Seismic fragility of Italian RC precast industrial structures. Engineering Structures 94: 122–36. doi: 10.1016/j. engstruct.2015.02.034

Castellazzi, G., Pantò, B., Occhipinti, G., Talledo, D. A., Berto, L., & Camata, G. (2021). A comparative study on a complex URM building: part II—issues on modelling and seismic analysis through continuum and discrete-macroelement models. Bulletin of Earthquake Engineering, 1-27.

Cattari S., Angiolilli M. (2022). Multiscale procedure to assign structural damage levels in masonry buildings from observed or numerically simulated seismic performance. Bulletin of Earthquake Engineering, under review.

Cattari, S., Camilletti, D., Lagomarsino, S., Bracchi, S., Rota, M., Penna, A. (2018). Masonry Italian code-conforming buildings. Part 2: nonlinear modelling and time-history analysis. Journal of Earthquake Engineering, 2010-2040.

Cattari, S., Degli Abbati, S., Ferretti, D., Lagomarsino, S., Ottonelli, D., Tralli, A. M. (2012). The seismic behaviour of ancient masonry buildings after the earthquake in Emilia (Italy) on May 20 and 29.

Cattari, S., Lagomarsino, S. (2009) A strength criterion for the flexural behaviour of spandrel in un-reinforced masonry walls. Proc. 14th WCEE, Beijing, China: 2008.

Cattari, S., Lagomarsino, S. (2013a). Analisi non lineari per la simulazione del danno di un fabbricato in San Felice sul Panaro (Emilia, 2012), in italian. Proceedings of XV Convegno ANIDIS "L'Ingegneria Sismica in Italia.

Cattari S, Lagomarsino S. (2013b) In: Sullivan T, Calvi G, editors. Masonry structures: In developments in the field of displacement-based seismic assessment. IUSS PRESS and EUCENTRE.

Cattari, S., Magenes, G. (2021) Benchmarking the software packages to model and assess the seismic response of unreinforced masonry existing buildings through nonlinear static analyses. Bull Earthquake Eng (2021). https://doi.org/10.1007/s10518-021-01105-0

Cattari, S., Angiolilli, M., Alfano, S., Brunelli, A., De Silva, F. (2022). Investigating the combined role of the structural vulnerability and site effects on the seismic response of a URM school hit by the Central Italy 2016 earthquake. Structures (Vol. 40, pp. 386-402).

Celik O.C., B.R. Ellingwood. Modeling beam-column joints in fragility assessment of gravity load designed reinforced concrete frames. Journal of Earthquake Engineering, 12(3), 357-381, 2008.

Cosenza E., Del Vecchio C., Di Ludovico M., Dolce M., Moroni C., Prota A., Renzi E. The Italian guidelines for seismic risk classification of constructions: technical principles and validation. Bulletin of Earthquake Engineering, 16, 5905-5935, 2018.

Croci G, Viskovic A, Herzalla A, Erdik M, Akdoğan M, de Canio G, Antonelli L (2010) Seismic assessment by numerical analyses and shaking table tests for complex masonry structures: the Hagia Irene case study. Adv Mater Res 133:777–782

D.M. 30/05/1972. Decreto Ministeriale 30 maggio 1972. Norme tecniche alle quali devono uniformarsi le costruzioni in conglomerato cementizio, normale e precompresso ed a struttura metallica. Gazzetta Ufficiale n. 190 del 22 luglio 1972.

D'Ayala, D. F., Paganoni, S. (2011). Assessment and analysis of damage in L'Aquila historic city centre after 6th April 2009. Bulletin of Earthquake Engineering, 9(1), 81-104.

De Felice G. (2011) Out-of-plane seismic capacity of masonry depending on wall section morphology, International Journal of Architectural Heritage, 5 (4-5),466-482.

De Risi M.T., M. Di Domenico, V. Manfredi, M. Terrenzi, G. Camata, F. Mollaioli, F. Noto, P. Ricci, P. Franchin, A. Masi, E. Spacone, G.M. Verderame. Modelling and seismic response analysis of pre-code and low-code reinforced concrete buildings in Italy. Part I: bare frames. Journal of Earthquake Engineering, 2022. (doi: 10.1080/13632469.2022.2074919).

De Risi M.T., P. Ricci, G.M. Verderame. Modelling exterior unreinforced beam-column joints in seismic analysis of non-ductile RC frames. Earthquake Engineering and Structural Dynamics, 46(6), 899-923, 2017.

De Risi MT, Di Domenico M, Ricci P, Verderame GM, Manfredi G. Experimental investigation on the influence of the aspect ratio on the in-plane/out-of-plane interaction for masonry infills in RC frames. Engineering Structures 2019;189:523-540.

Decanini L.D., G.E. Fantin. Modelos simplificados de la mampostería incluidas en porticos. Características de rigidez y resistencia lateral en estado límite. Actas de las VI Jornadas Argentinas de Ingenieria Estructural, Buenos Aires, Argentina, October 1–3, 1986. (in Spanish)

Decanini L.D., L. Liberatore, F. Mollaioli. Strength and stiffness reduction factors for infilled frames with openings. Earthquake Engineering and Engineering Vibration, 13(3), 437– 454, 2014.

Degli Abbati, S., Morandi, P., Cattari, S., & Spacone, E. (2021). On the reliability of the equivalent frame models: the case study of the permanently monitored Pizzoli's town hall. Bulletin of Earthquake Engineering, 1-31.

Del Gaudio C, De Risi MT, Verderame GM. Seismic loss prediction for infilled RC buildings via simplified analytical method. Journal of Earthquake Engineering, 2021 (in press).

Del Gaudio C., M.T. De Risi, P. Ricci, G.M. Verderame. Empirical drift-fragility functions and loss estimation for infills in reinforced concrete frames under seismic loading. Bulletin of Earthquake Engineering, 17(3), 1285-1330, 2019.

Del Gaudio C., P. Ricci, G.M. Verderame. A class-oriented mechanical approach for seismic damage assessment of RC buildings subjected to 2009 L'Aquila earthquake. Bulletin of Earthquake Engineering 2018, 16, 4581-4605.

Demartino C., Vanzi I., Monti G., Sulpizio C. (2018). Precast industrial buildings in Southern Europe: loss of support at frictional beam-to-column connections under seismic actions. Bulletin of Earthquake Engineering, 16(1):259-294

Di Domenico M., M.T. De Risi, P. Ricci, G.M. Verderame, G. Manfredi. Empirical prediction of the in-plane/out-of-plane interaction effects in clay brick unreinforced masonry infill walls. Engineering Structures, 227, 2021d.

Di Domenico M., M.T. De Risi, V. Manfredi, M. Terrenzi, G. Camata, F. Mollaioli, F. Noto, P. Ricci, P. Franchin, A. Masi, E. Spacone, G.M. Verderame. Modelling and seismic response analysis of pre-code and low-code reinforced concrete buildings in Italy. Part II: infilled frames. Journal of Earthquake Engineering, 2022. (doi: 10.1080/13632469.2022.2086189).

Di Domenico M., P. Ricci, G.M. Verderame. Empirical calibration of hysteretic parameters for modelling the seismic response of reinforced concrete columns with plain bars. Engineering Structures, 237, 2021a.

Di Domenico M., P. Ricci, G.M. Verderame. Floor spectra for bare and infilled reinforced concrete buildings designed according to Eurocodes. Earthquake Engineering and Structural Dynamics, 2021b, 50(13), 3577-3601.

Di Ludovico, M., A. Prota, C. Moroni, G. Manfredi, and M. Dolce (2017a). Reconstruction process of damaged residential buildings outside historical centres after the L'Aquila earthquake: Part I —"light damage" reconstruction. Bulletin of Earthquake Engineering 15 (2): 667–92.

Di Ludovico, M., A. Prota, C. Moroni, G. Manfredi, and M. Dolce (2017b) Reconstruction process of damaged residential buildings outside historical centres after the L'Aquila earthquake: Part II —"heavy damage" reconstruction. Bulletin of Earthquake Engineering 15 (2): 693–729.

Dolce, M., Speranza, E., Giordano, F., Borzi, B., Bocchi, F., Conte, C., Di Meo, A., Faravelli, M., Pascale, V. (2019). Observed damage database of past Italian earthquakes: the Da. DO WebGIS. Bollettino di Geofisica Teorica ed Applicata, 60(2).

DT212 (2013). Tecnichal Documentation of the National Research Council (CNR). Guide for the Probabilistic assessment of the seismic safety of existing buildings, Available at: https://www.cnr.it/en/node/2643.

Ercolino, M., Magliulo, G., Manfredi, G. (2016). Failure of a precast RC building due to Emilia-Romagna earthquakes. Engineering Structures, 118, 262-273

Esposito R, Messali F, Ravenshorst GJP, Shipper HR, Rots JG (2019) Seismic assessment of a lab-tested two-storey unreinforced masonry Dutch terraced house. Bull Earthq Eng 17:4601–4623

Eteme Minkada, M., Labò, S., Marini, A., Belleri, A. (2021). Preliminary considerations on the loss of support for precast beam elements. COMPDYN 2021, Athens, Greece, 27–30 June 2021.

Eurocode 2. Design of Concrete Structures. Part 1-1: General Rules and Rules for Buildings. Brussels, 2004.

Eurocode 8. Design of structures for Earthquake Resistance. Part 1-1: General Rules, Seismic Actions and Rules for Buildings. Brussels, 2004.

Evangelista L., S. del Gaudio, C. Smerzini, A. d'Onofrio, G. Festa, I. Iervolino, L. Landolfi, R. Paolucci, A. Santo, F. Silvestri. Physics-based seismic input for engineering applications: a case study in the Aterno river valley, Central Italy. Bulletin of Earthquake Engineering, 15, 2645–2671, 2017.

Furtado, A., Rodrigues, H., Arêde, A., Varum, H., Grubišić, M., Šipoš, T. K. (2018). Prediction of the earthquake response of a three-storey infilled RC structure. Engineering Structures, 171, 214-235.

Gajera K, Dal Lago B, Capacci L, Biondini F. (2021). Multi-Stripe Seismic Assessment of Precast Industrial Buildings With Cladding Panels. Front. Built Environ. 7:631360. Doi: 10.3389/fbuil.2021.631360

Graziotti, F., Guerrini, G., Rossi, A., Andreotti, G., Magenes, G. (2018). Proposal for an improved procedure and interpretation of ASTM C1531 for the in situ determination of brick-masonry shear strength. Masonry.

Graziotti, F., Magenes, G., Penna, A. (2012) Experimental cyclic behaviour of stone masonry spandrels. Proc. of the 15th World Conference on Earthquake Engineering. Lisboa. PT.

Grünthal, G. (1998). Cahiers du Centre Européen de Géodynamique et de Séismologie: Volume 15–European Macroseismic Scale 1998. European Center for Geodynamics and Seismology, Luxembourg.

Haselton C.B. and Deierlein G.G. Benchmarking Seismic Performance of Reinforced Concrete Frame Buildings. Structures Congress 2005, April 20-24, New York, United States, 2005.Iervolino, I., Spillatura, A., Bazzurro, P. (2018) Seismic reliability of Code-Conforming Italian Buildings, Journal of Earthquake Engineering, 22, sup2, 5-27.

Haselton C.B., Liel A.B., Taylor-Lange S., Deierlein G.G. [2008] "Beam-column element model calibrated for predicting flexural response leading to global collapse of RC frame buildings", PEER Report No. 2007/03. Pacific Earthquake Engineering Research Center, University of California, Berkeley, CA, USA.

Iervolino, I., R. Baraschino, and A. Spillatura. [2021]. Evolution of seismic reliability of code-conforming Italian buildings. Journal of Earthquake Engineering (submitted)

Iervolino, I., Spillatura, A., Bazzurro, P. (2018). Seismic reliability of code-conforming Italian buildings. Journal of Earthquake Engineering, 22(sup2), 5-27.

Indirli, M., Kouris, L.A. S., Formisano, A. Borg, R.P., Mazzolani F.M., (2013) Seismic Damage Assessment of Unreinforced Masonry Structures After The Abruzzo 2009 Earthquake: The Case Study of the Historical Centers of L'Aquila and Castelvecchio Subequo, International Journal of Architectural Heritage, 7:5, 536-578, DOI: 10.1080/15583058.2011.654050

Kajiwara K., Tosauchi Y., Kang J.-D., Fukuyama K., Sato E., Inoue T., Kabeyasawa T., Shiohara H., Nagae T., Kabeyasawa T., Fukuyama H., Mukai T. Shaking-table tests of a full-scale ten-story reinforced-concrete building (FY2015). Phase I: Free-standing system with base sliding and uplifting. Engineering Structures 2021, 233.

Lagomarsino S., Cattari S., Angiolilli M., Bracchi S., Rota M., Penna A. (2022). Modelling and seismic response analysis of existing URM structures. Part 2: archetypes of Italian historical buildings. Journal earthquake engineering. Under review

Lagomarsino, S., Penna, A., Galasco, A., Cattari, S. (2013). TREMURI program: an equivalent frame model for the nonlinear seismic analysis of masonry buildings. Engineering structures, 56, 1787–1799.

Law n. 1684 25/11/1962. Gazzetta Ufficiale della Repubblica Italiana 22 dicembre 1962, n. 326. 1962 (in Italian).

Liberatore, L., Noto, F., Mollaioli, F., Franchin, P (2018). In-plane response of masonry infill walls: Comprehensive experimentally-based equivalent strut model for deterministic and probabilistic analysis. Engineering Structures, 167, 533–548, 2018.

Lourenço P.B., Leite J.M., Paulo-Pereira M.F., Campos-Costa A., Candeias P.X., Mendes N. (2016) Shaking table testing for masonry infill walls: unreinforced versus reinforced solutions. Earthquake Engineering and Structural Dynamics, 45:2241-2260.

Magenes, G., Penna, A., Galasco, A., da Pare´, M. (2010) In-plane cyclic shear tests of undressed double leaf stone masonry panels. In: 8th international masorny conference, Dresden, Germany, pp 1–10.

Magenes, G., Penna, A., Senaldi, I.E., Rota, M., Galasco, A. (2014) Shaking table test of a strengthened full-scale stone masonry building with flexible diaphragms, International Journal of Architectural Heritage, 8(3), 349-375.

Magliulo G, Di Salvatore C, Ercolino M. (2021). Modeling of the Beam-To-Column Dowel Connection for a Single-Story RC Precast Building. Front. Built Environ. 7: 627546. Doi: 10.3389/fbuil.2021.627546

Magliulo, G., Ercolino, M., Petrone, C., Coppola, O., Manfredi, G. (2014). The Emilia earthquake: seismic performance of precast reinforced concrete buildings. Earthquake Spectra, 30(2), 891–912. doi: 10.1193/091012EQS285M

Manfredi, Gaetano, Prota, Andrea, Verderame, Gerardo Mario, F. De Luca, Ricci, Paolo (2014). 2012 Emilia Earthquake, Italy: reinforced concrete buildings response. Bulletin of Earthquake Engineering, Vol. 12, P. 2275-2298, ISSN: 1570-761x, DOI: 10.1007/S10518-013-9512-X

Masi, A., Chiauzzi, L., Santarsiero, G., Manfredi, V., Biondi, S., Spacone, E., Del Gaudio, C., Ricci, P., Manfredi, G., Verderame, G. M. (2019). Seismic response of RC buildings during the Mw6.0 august 24, 2016 Central Italy earthquake: The Amatrice case study. Bulletin of Earthquake Engineering, Vol. 17, P. 5631-5654, ISSN: 1570-761x, DOI: 10.1007/S10518-017-0277-5

McKenna F., G.L. Fenves, M.H. Scott. Open system for earthquake engineering simulation. University of California, Berkeley, CA, 2000.

Mendes N, Costa AA, Louren.o PB, Bento R, Beyer K, de Felice G, Gams M, Griffith M, Ingham JM, Lagomarsino S, Lemos JV, Liberatore D, Modena C, Oliveira DV, Penna A, Sorrentino L (2017) Methods and approaches for blind test predictions of out of-plane behavior of masonry walls: a numerical comparative study. Int J Architect Herit 11(1):59–71

Minghini, F., Ongaretto E., Ligabue V., Savoia M., Tullini N. (2016). Observational failure analysis of precast buildings after the 2012 Emilia earthquakes. Earthquakes and Structures 11(2): 327–46. doi:10.12989/eas.2016.11.2.327

MIT (2019). Ministry of Infrastructures and Transportation, Circ. C.S.Ll.PP. No. 7 of 21/1/2019. Istruzioni per l’applicazione dell’aggiornamento delle norme tecniche per le costruzioni di cui al Decreto Ministeriale 17 Gennaio 2018, Technical Document, in italian.

Morandi, P., Manzini, C.F., Magenes, G. (2019) Application of seismic design procedures on three modern URM buildings struck by the 2012 Emilia earthquakes: inconsistencies and improvement proposals in the European codes. Bull Earthquake Eng, 18, 547-580.

Nastri, E., Vergato M., Latour, M. (2017). Performance evaluation of a seismic retrofitted R.C. precast industrial building. Earthquakes and Structures 12(1). doi: 10.12989/eas.2017.12.1.013

Noh N.M., L. Liberatore, F. Mollaioli, S. Tesfamariam. Modelling of masonry infilled RC frames subjected to cyclic loads: State of the art review and modelling with OpenSees. Engineering Structures 150, 599–621, 2017.

NTC (2018). Norme tecniche per le costruzioni. Ministero delle Infrastrutture e dei Trasporti, Technical Document, in italian.

Ottonelli D, Marano C, Manzini C, Calderoni B, Cattari S (2021) A comparative study on a complex URM building. Part I: sensitivity of the seismic response to different modelling options in the equivalent frame models. Bulletin of Earthquake Engineering, https://doi.org/10.1007/s10518-021-01128-7.

Ottonelli, D., Cattari, S., Lagomarsino, S. (2020). Displacement-Based Simplified Seismic Loss Assessment of Masonry Buildings. Journal of Earthquake Engineering, 24(sup1), 23-59.

Palanci, M., Senel, S. M., and Kalkan, A. (2017). Assessment of one story existing precast industrial buildings in Turkey based on fragility curves. Bull. Earthq. Eng. 15 (1), 271–289. doi:10.1007/s10518-016-9956-x

Parisse, F., Cattari, S., Marques, R., Lourenço, P.B. Magenes, G., Beyer, K. , Calderoni, B. Camata, G. , Cordasco, E.A. , Erberik, M.A. İçel, C. , Karakaya, M., Malomo, D., Manzini, C.F. , Marano, C. Messali, F. , Occhipinti, G. , Pantò, B., Saygılı, Ö. , Sousamli, M. (2021) Benchmarking the seismic assessment of unreinforced masonry buildings from a blind prediction test, Structures 31, 982-1005. https://doi.org/10.1016/j.istruc.2021.01.096.

Penna, A., Morandi, P., Rota, M., Manzini, C. F., Da Porto, F., Magenes, G. (2014). Performance of masonry buildings during the Emilia 2012 earthquake. Bulletin of Earthquake Engineering, 12(5), 2255-2273.

Penna, A., Rota, M., Bracchi, S., Angiolilli, M., Cattari, S., Lagomarsino, S. (2022), Modeling and seismic response analysis of existing URM structuress. Part 1: modern buildings, submitted to Journal of Earthquake Engineering.

Rezaie, A., Godio, M., Beyer, K. (2020). Experimental investigation of strength, stiffness and drift capacity of rubble stone masonry walls. Construction and Building Materials, 251, 118972.

Ricci P, Di Domenico M, Verderame GM 2018a. Experimental assessment of the in-plane/out-of-plane interaction in unreinforced masonry infill walls. Engineering Structures 2018b;173:960-978.

Ricci P, Di Domenico M, Verderame GM. Effects of the in-plane/out-of-plane interaction in URM infills on the seismic performance of RC buildings designed to Eurocodes. Journal of Earthquake Engineering, 2020 (in press).

Ricci P., M. Di Domenico, G. M. Verderame. Empirical-based out-of-plane URM infill wall model accounting for the interaction with in-plane demand. Earthquake Engineering and Structural Dynamics, 47(3), 802-827, 2018.

Ricci, P., De Luca, F., Verderame, G. M. (2011). 6th April 2009 L'Aquila earthquake, Italy: reinforced concrete building performance. Bulletin of earthquake engineering, 9(1), 285-305.

Richard, B., Martinelli, P., Voldoire, F., Chaudat, T., Abouri, S., Bonfils, N. (2016). SMART 2008: Overview, synthesis and lessons learned from the International Benchmark. Engineering Structures, 106, 166-178.

Rota, M., Penna, A., & Strobbia, C. L. (2008). Processing Italian damage data to derive typological fragility curves. Soil Dynamics and Earthquake Engineering, 28, 933–947.

Savoia M., Mazzotti C., Buratti N., Ferracuti B., Bovo M., Ligabue V. (2012). Damages and collapses in industrial precast buildings after the Emilia earthquake. Ingegne. Sismi. 29, 120–131

Schoettler, M. J., Belleri, A., Dichuan, Z., Restrepo, J. I., Fleischman, R. B. (2009). Preliminary results of the shake-table testing for the development of a diaphragm seismic design methodology. PCI journal, 54(1), 100-124.

Senaldi,I.E., Guerrini, G., Comini, P., Graziotti, F., Penna, A., Beyer, K., Magenes, G. (2020) Experimental seismic performance of a half-scale stone masonry building aggregate, Bulletin of Earthquake Engineering, 18(2), 609-643.

SERA Project – Seismic Testing of Adjacent Interacting Masonry Structures (2017) Blind prediction of a shake table test on a masonry building aggregate, https://doi.org/10.5281/zenodo.3445391

Sorrentino, L., Cattari, S., Da Porto, F., Magenes, G., Penna, A. (2019). Seismic behaviour of ordinary masonry buildings during the 2016 central Italy earthquakes. Bulletin of Earthquake Engineering, 17(10), 5583-5607.

Sousa R, Batalha N, Silva V, Rodrigues H. (2020). Seismic fragility functions for Portuguese RC precast buildings. Bull Earthquake Eng. https://doi.org/10.1007/s10518-020-01007-7

Spina, D., Acunzo, G., Fiorini, N., Mori, F., Dolce, M. (2019). A probabilistic simplified seismic model of masonry buildings based on ambient vibrations. Bulletin of Earthquake Engineering, 17(2), 985-1007.

Toniolo G., Colombo A. (2012). Precast concrete structures: the lessons learned from the L'Aquila earthquake. Structural Concrete, 13(2):73-83

Turnšek, V., Sheppard, P. (1980). The shear and flexural resistance of masonry walls. In proc. int. research conference on earthquake engineering, (pp. 517-573). Skopje, Japan.

Vanin, F., Zaganelli, D., Penna, A., Beyer, K. (2017). Estimates for the stiffness, strength and drift capacity of stone masonry walls based on 123 quasi-static cyclic tests reported in the literature. Bulletin of Earthquake Engineering, 15, 5435–5479.

Verderame G.M., De Luca F., Ricci P., Manfredi G. (2011). Preliminary analysis of a soft-storey mechanism after the 2009 L'Aquila earthquake. Earthquake Engineering & Structural Dynamics, Vol. 40, P. 925-944, John Wiley & Sons, ISSN: 0098-8847, DOI: 10.1002/Eqe.1069

Verderame G.M., Ricci P. [2018] "An empirical approach for nonlinear modelling and deformation capacity assessment of RC columns with plain bars", *Engineering Structures*, 176, 539-554.

Vicente RS, Rodrigues H, Varum H et al. Performance of masonry enclosure walls: lessons learned from recent earthquakes. Earthquake engineering and engineering vibration 2012;11.1:23-34.

Xiao, J., Pham, T. L., Ding, T. (2015). Shake table test on seismic response of a precast frame with recycled aggregate concrete. Advances in Structural Engineering, 18(9), 1517-1534.

Yeow T.Z., K. Kusunoki, I. Nakamura, Y. Hibino, T. Ohkubo, T. Seike, S. Yagi, T. Mukai, P. Calvi, M. Moustafa, S. Fukai. The 2019 Tokyo Metropolitan Resilience Project E-Defense Test of a 3-story Disaster Management Center. Proceedings of the 17$^{th}$ World Conference on Earthquake Engineering, 17WCEE. Sendai, Japan, September 13$^{th}$-18$^{th}$ 2020.

Zhang, D., Fleischman, R. B., Schoettler, M. J., Restrepo, J. I., Mielke, M. (2019). Precast Diaphragm Response in Half-Scale Shake Table Test. Journal of Structural Engineering, 145(5), 04019024.